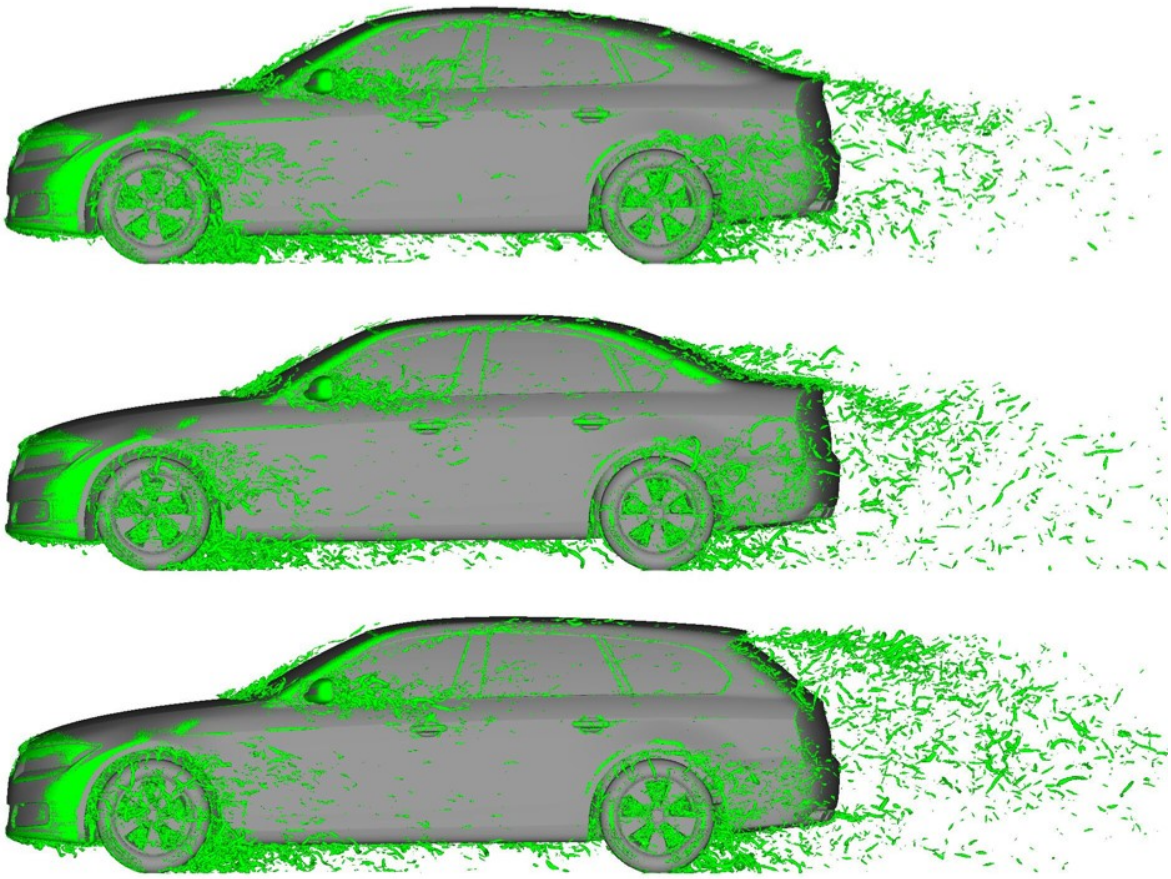

Steady and Unsteady Numerical Analysis of the DrivAer Model

Master's thesis in Applied Mechanics

RAMAN YAZDANI

Department of Applied Mechanics
CHALMERS UNIVERSITY OF TECHNOLOGY
Göteborg, Sweden 2015

MASTER'S THESIS IN APPLIED MECHANICS

Steady and Unsteady Numerical Analysis of the DrivAer Model

RAMAN YAZDANI

Department of Applied Mechanics
Division of Vehicle Engineering and Autonomous Systems
CHALMERS UNIVERSITY OF TECHNOLOGY

Göteborg, Sweden 2015

Steady and Unsteady Numerical Analysis of the DrivAer Model
RAMAN YAZDANI

Master's thesis 2015:34
ISSN 1652-8557
Department of Applied Mechanics
Division of Vehicle Engineering and Autonomous Systems
Chalmers University of Technology
SE-412 96 Göteborg
Sweden
Telephone: +46 (0)31-772 1000

Cover:
Illustration of separation zones on the fastback, notchback, and squareback version of the DrivAer model

Chalmers Reproservice
Göteborg, Sweden 2015

Steady and Unsteady Numerical Analysis of the DrivAer Model
Master's thesis in Applied Mechanics
RAMAN YAZDANI
Department of Applied Mechanics
Division of Vehicle Engineering and Autonomous Systems
Chalmers University of Technology

Abstract

This work consists of steady and unsteady numerical analysis of the DrivAer vehicle model. The CAD model is free for anyone to use and is setting the new standard for benchmarking numerical analysis against experimental data in academia and industry. The model consists of a standardised car with interchangeable rear ends, resulting in a fastback, notchback, and squareback model. The models can be analysed with flat or detailed underbody and with or without closed wheelhouses, resulting in no wheels.

A comparison of the numerical results and experimental results has been performed using test data from scale model testing at TU München and TU Berlin, and full scale testing at Volvo Cars performed by Ford of Europe and made available to the author. The numerical analysis consists of three different methods, first a steady-state method using the realisable $k-\epsilon$ turbulence model with standard wall treatment and a mesh consisting of 50 million cells for a full car simulation. Second, a similar method as the first one except for a refined mesh using six prism layers, resulting in 200 million cells and combining this with enhanced wall treatment. Finally a unsteady delayed detached eddy simulation, DDES, method with Spalart Allmaras, SA, turbulence modelling is used combined with the same mesh in the second method mentioned.

The results of this work show that the unsteady method has a better capability of predicting drag force trends, surface pressure distribution at the base, and flow field behaviour in the wake. While the steady-state method with enhanced wall treatment shows good ability to predict absolute drag values for the detailed underbody, the unsteady method show similar abilities but excels in many different configurations when in comparison.

Keywords: DrivAer, CFD, VCC, CTH, TUM, TUB, Ford, Steady-State, Realisable $k-\epsilon$, Unsteady, SA-DDES, ANSA, FLUENT, ENSIGHT

Preface

In this work, steady and unsteady numerical analysis has been performed on the DrivAer model. The analysis has been conducted by one student from January 2015 to June 2015 at Volvo Cars Aerodynamics group. The work is part of a method development project at Volvo Cars where several methods and software for computational fluid dynamics are evaluated. Methods used in this work have been developed in cooperation with the Department of Applied Mechanics, Vehicle Engineering and Autonomous Systems, VEAS, Chalmers University of Technology, Sweden.

Many thanks to my examiner Professor Lennart Löfdahl, supervisor Adjunct Professor Simone Sebben, Dr. Lennert Sterken, and the staff at Volvo Cars aerodynamics group for all the support during the project. Finally Ford of Europe, TU München, and TU Berlin can not be thanked enough for all the experimental data made available for this work.

Göteborg June 2015
RAMAN YAZDANI

Nomenclature

C_d	Drag coefficient
C_p	Pressure coefficient
C_{p-tot}	Total pressure coefficient
C_μ	Turbulent viscosity constant
ε	Turbulent dissipation equation
f_d	DES Limiter
k	Turbulent kinetic energy equation
k_{mod}	Modelled turbulent kinetic energy
k_{res}	Resolved turbulent kinetic energy
v	velocity in x direction, $[m/s]$
ν	Kinematic viscosity, $[m^2/s]$
ν_t	Eddy viscosity, $[m^2/s]$
μ	Viscosity, $[m^2/s]$
U_∞	Free stream velocity, $[m]$
y_+	Dimensionless wall distance

CFD	Computational Fluid Dynamics
$RANS$	Reynolds Averaged Navier Stokes
$SA-DDES$	Spalart Allmaras - Delayed Detached Eddy Simulation
$URANS$	Unsteady Reynolds Averaged Navier Stokes

Contents

Figures

1 Introduction

Benchmarking numerical methods for estimating aerodynamic behaviour of cars has in the past been not appropriate for the automotive industry due to the lack of complexity in the available generic models. Models such as the Ahmed body or the SAE body have to little resemblance to a modern car and is thus inherently not as useful for industry as it can be for research. The recently developed DrivAer model [1] offers a reasonable amount of detail and is based on car models from Audi and BMW. The DrivAer model is open for anyone to use which creates a new domain for benchmarking numerical methods between companies in the automotive industry.

Previous work on the DrivAer model greatly consists of experimental data on scale models used in the wind tunnel at TU München [1, 2] and TU Berlin [3, 4]. In general there are only a few publications on the topic since the model was created in 2012 but some recent numerical results can be found in [5] and [6].

To be able to compare their standard and future methods Volvo Cars has together with Chalmers University of Technology decided to conduct a extensive numerical investigation of the DrivAer model, which results in this masters thesis.

Problems discussed are the correlation between numerical and experimental data and the differences between the methods used to generate the numerical data.

1.1 Purpose

The purpose of the project is to benchmark the standard procedure for steady numerical analysis used at Volvo Cars [7], a method for unsteady analysis [8, 9], and a mix of them two using the mesh from the unsteady method in steady analysis with enhanced wall treatment. The main focus will lie in investigating how well the three numerical methods correlate with experimental results in the regard of drag prediction, trends, and flow field behaviour. Front and rear lift forces are not included within the scope of this work due to the lack of experimental data made available.

1.2 Limitations

The project is limited to numerical analysis only. The experimental data used is based on previous work done at TU München [1, 2], TUM, TU Berlin [3, 4], TUB, and limited data from the Volvo wind tunnel, PVT, provided by Ford of Europe. The accuracy of the TUM data is slightly inferior when compared to the PVT data, due to the scale wind tunnel lacking the same sophistication in boundary layer control and moving ground simulation. The PVT data is full-scale using ground effect simulation system [10], but is limited to two different configurations. The data from TUB has been generated without a moving ground system which will impact the results.

The study is limited to only comparing drag forces, the lift forces will be disregarded due to limited amount of lift data and known difficulties from TUM in reproducing lift forces. Finally the project is time limited to one persons work for 20 weeks.

1.3 Method

The methods used in the project is based on the current and developing methods for steady [7] and unsteady [8] numerical analysis at Volvo Cars. The outline of the method is that different mesh strategies are implemented in the mesh generator Harpoon. The mesh is then imported into the CFD solver Fluent and after solving, post-processed in Ensight. The whole process is automated using Python scripts, enabling the user to focus on generating configurations and analysing them.

2 Theory

The problem of estimating drag and lift forces on a vehicle using numerical methods is solving Navier-Stokes equation. This equation remain unsolved yet today and various methods of estimating the solution has thus been developed over the years. The equation is composed of the continuity- and momentum equation and for incompressible flow with constant viscosity, non-conservative form, follows

$$\rho\frac{\partial v_i}{\partial t} + \rho v_j\frac{\partial v_i}{\partial x_j} = -\frac{\partial p}{\partial x_i} + \mu\frac{\partial^2 v_i}{\partial x_j \partial x_j} \tag{2.1}$$

where ρ denotes density, v velocity, t time, x position, p pressure, and μ viscosity.

2.1 Solving

Almost all fluid flow connected to vehicles is turbulent. The turbulent flow is usually divided in two parts, a time-averaged part $\bar{v}_i$, and a fluctuating part $v_i^{'}$ so that $v_i = \bar{v}_i + v_i^{'}$. Turbulence is not defined but it has six characteristic features, irregularity, diffusivity, large Reynolds numbers, three-dimensional, dissipative, and the turbulent flow can be treated as a continuum.

2.1.1 Steady

In order to obtain an estimate solution to the Navier-Stokes equation a numerical method combined with a turbulence model is used. The steady method used in the work is Reynolds-Averaged Navier-Stokes, RANS, combined with the $k-\epsilon$ turbulence model. This can be classified as an turbulent viscosity model based on the Boussinesq assumption. In the Boussinesq assumption a turbulent viscosity is introduced to model the unknown Reynolds Stresses in Navier-Stokes equation. The $k-\epsilon$ model is generated by inserting model assumptions for the turbulent diffusion, the production, and the buoyancy term into the k and ϵ equations. Where the k and ϵ equations stands for turbulent kinetic energy equation and turbulent dissipation equation, both derived from Navier-Stokes equation 2.1.

2.1.2 Unsteady

The unsteady numerical method is based on Delayed Detached Eddy Simulation, DDES, methodology using the Spalart-Allmaras, SA, turbulence model. The model is an modification of the original DES97 model with an introduction of a limiter f_d, see [9] for further description of the SA-DDES method. Detached Eddy Simulation, DES is a mix of Large Eddy Simulation, LES, and Unsteady Reynolds-Averaged Navier-Stokes, URANS. The model treats the boundary layer with URANS and capture the outer detached eddies with LES. The limiter f_d is used to ensure that the model will not switch to LES mode in the boundary layer. The limiter is defined as:

$$f_d = 1 - tanh((8r_d)^3) \tag{2.2}$$

where:

$$r_d = \frac{v_t + v}{\sqrt{U_{i,j}U_{i,j}\kappa^2 d^2}} \tag{2.3}$$

Equation 2.3 is composed of the turbulent kinematic viscosity v_t, molecular viscosity v, velocity gradient $U_{i,j}$, von-kármán constant κ, and the wall distance d. The limiter function is 1 in the LES regions and transitions smoothly to 0 in the boundary layer, URANS regions.

2.2 Post-processing

Some useful entities used during the post-processing of data in this work are drag force coefficient, pressure coefficient, total pressure coefficient, and velocity streamlines. The equations describing these are found below:

$$C_d = \frac{F_X}{1/2\rho U_\infty^2 A} \tag{2.4}$$

where F_X is the total force in X, u_∞ the free stream velocity, and A the frontal area of the vehicle.

$$C_p = \frac{p - p_\infty}{1/2\rho u_\infty^2} \tag{2.5}$$

$$C_{p-tot} = C_p + \frac{v^2}{u_\infty^2} \tag{2.6}$$

where p is the pressure, p_∞ is the free stream pressure, and v is the velocity. For evaluation of the DDES performance the modelled and resolved turbulent kinetic energy is calculated using the equations below. The non-dimensional resolved turbulent kinetic energy, k_{res}, is obtained using:

$$\frac{< u^2 v^2 w^2 >}{2U_\infty} \tag{2.7}$$

The modelled turbulent kinetic energy is approximated in the SA-DDES model as:

$$\frac{\nu_t \sqrt{2S_{ij}S_{ij}}}{U_\infty^2 \sqrt{C_\mu}} \tag{2.8}$$

where ν_t is turbulent kinematic viscosity, S_{ij} the strain-rate tensor, and C_μ the turbulent viscosity constant.

3 Methodology

The methodology of the CFD simulations can be divided into four sections for the three different procedures, geometry preparation, volume meshing, solving, and post-processing. Four different commercial software are used in the processes. ANSA - geometry preparation, HARPOON - volume meshing, FLUENT - solving, and ENSIGHT - post-processing. It is important to denote that choosing methods for the numerical simulations is not within the scope of this work, the purpose is only to evaluate the procedures developed at Volvo Cars.

3.1 Geometry

The DrivAer vehicle model consists of three different rear ends, fastback, figure 3.1a, notchback, figure 3.1b, and squareback, figure 3.1c. Only the top rear end, tophat, is interchangeable, thus leaving the underbody and front/mid part of the model the same. The configuration denoted baseline, figure 3.1d and A.1a, consists of the three different models with closed front, meaning entirely closed engine compartment, wheels, slick tires, mirrors, and detailed underbody. Smooth underbody, figure 3.1e and A.1b, denotes the same configuration as baseline except for a completely smooth underbody. The closed body, figure 3.1f and A.1c, configuration consists of the smooth underbody configuration without wheels and has completely closed wheel arches and underbody. The three different underbody configurations are used on the three different rear ends, resulting in nine different configurations within the scope of this work.

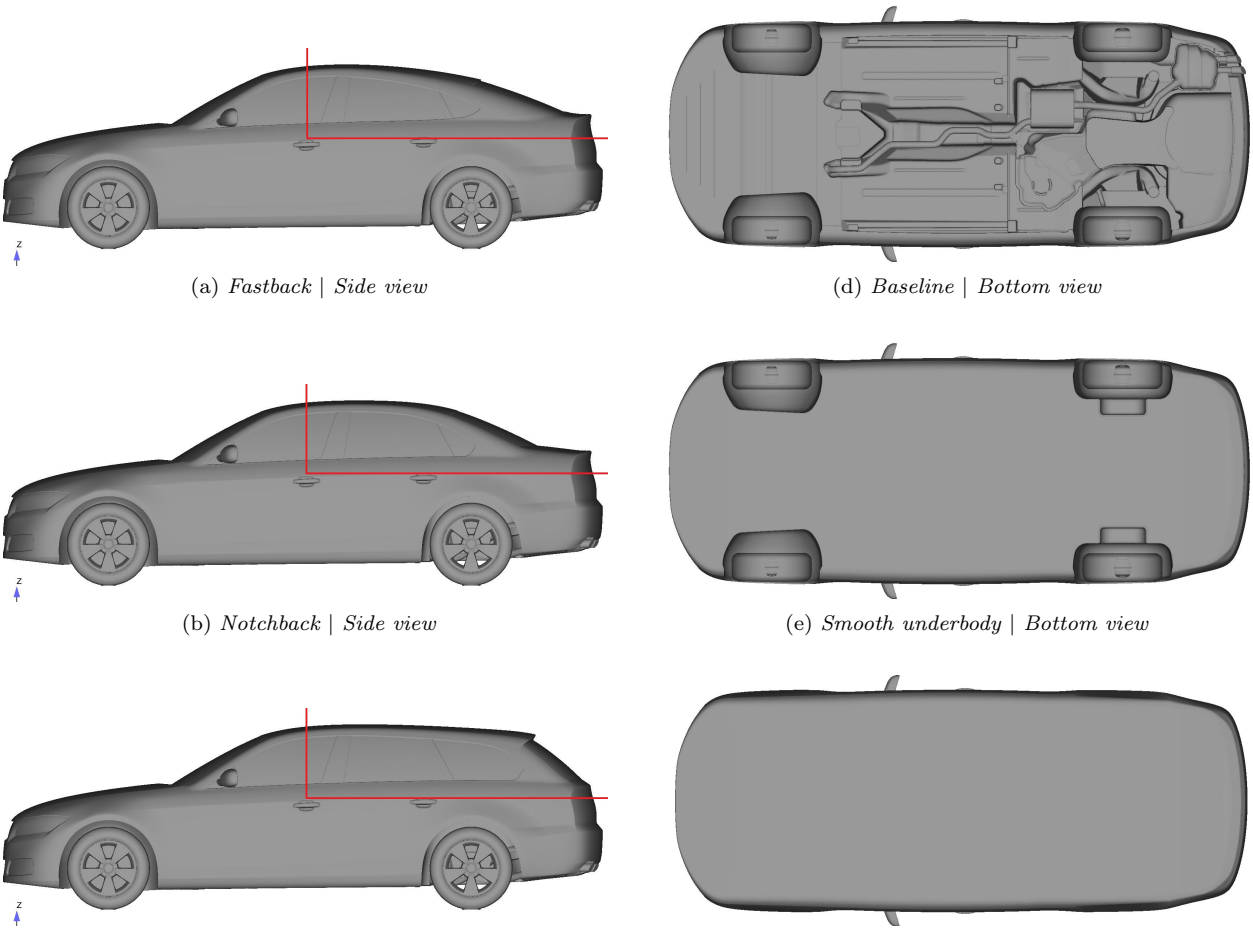

(a) *Fastback | Side view*

(d) *Baseline | Bottom view*

(b) *Notchback | Side view*

(e) *Smooth underbody | Bottom view*

(c) *Squareback | Side view*

(f) *Closed body | Bottom view*

Figure 3.1: *Geometry and configurations*

3.2 Mesh generation

Mesh generation is the creation of a volume net describing the vehicle and the domain. The key properties of the mesh is cell type, surface cell size, cell growth in the volume, refinement boxes in the volume, and domain size. Common for both the steady and unsteady simulation is the cell type and domain size. Hexahedral cells are used in both procedures for their robustness and ease of control when adjusting cell growth rates in the volume. The domain size is $50x10x10m$, and the front of the car is positioned at $15m$ from the inlet, which means roughly three car lengths in front of the vehicle and six car lengths behind the vehicle. Further details are found in [7].

During geometry preparation in ANSA, the model is divided into different surface regions. This division enables the user to set surface cell size, prism layers, and expansions, based on specific surface regions. The same division of surface regions is used for all simulations and can be seen in figure 3.2.

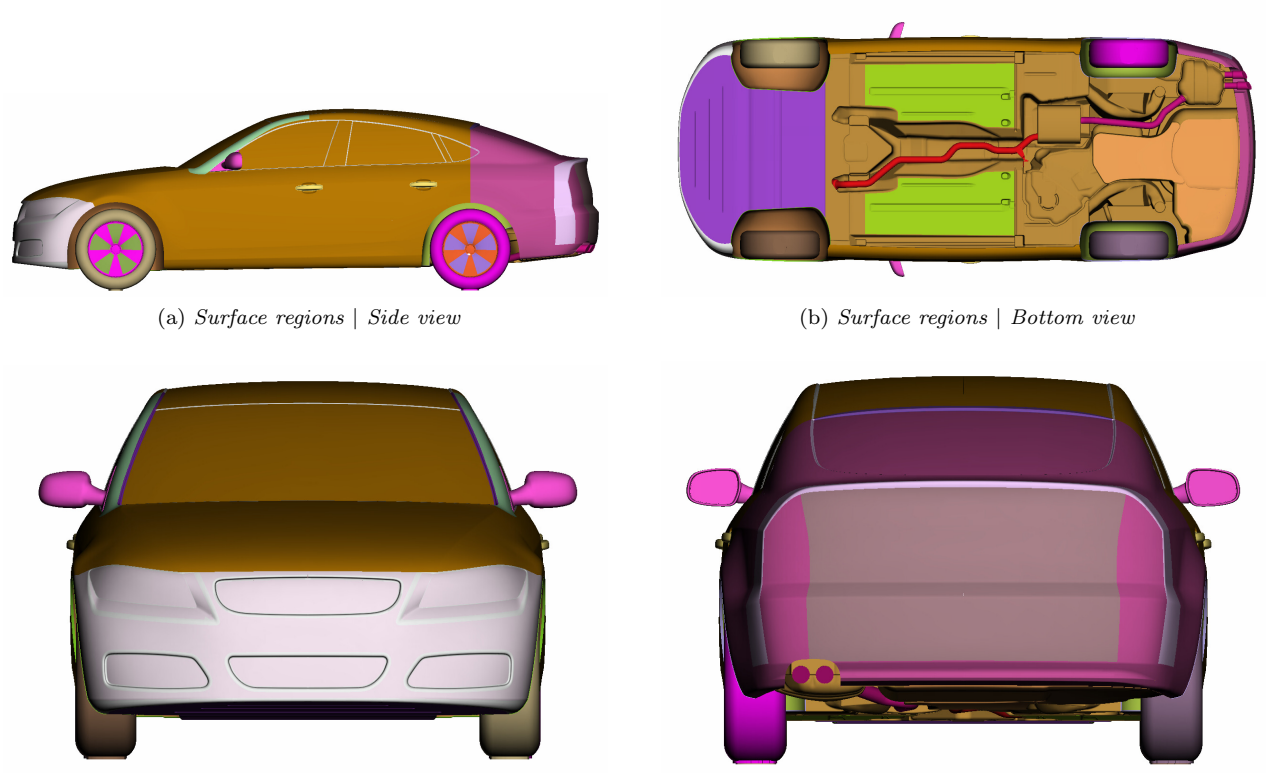

(a) *Surface regions | Side view*

(b) *Surface regions | Bottom view*

(c) *Surface regions | Front view*

(d) *Surface regions | Rear view*

Figure 3.2: *Division of surface regions for mesh adaptability*

The surface cell size of the steady mesh varies from $1.25mm$ to $5mm$ and between $1.5mm$ to $6mm$ for the steady enhanced wall treatment and unsteady mesh. The smaller cell size is naturally used at areas such as front region, spoiler, tail lights and radii. The unsteady mesh utilises prism layers on certain areas of the underbody and radii at the top, this is combined with expansion ratios to reach smooth transitions in the volume. The prism layers consist of 6 layers and are designed to reach a $y^+ = \frac{u_* y}{v}$ of 20, where u_* is the friction velocity at the nearest wall, y the distance to the nearest wall, and v the local kinematic viscosity, resulting in a first layer height of $0.6mm$, which is further described in [8]. Prism layers are not used in the steady mesh but expansion ratios are adjusted in some surface regions. Further details about the surface regions, surface cell size, and expansion ratios can be found in [7].

Refinement boxes are used in order to increase the mesh density in regions as, wake, mirrors, underbody etc. The refinement boxes are illustrated in figure 3.3.

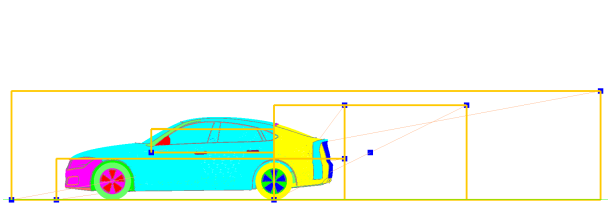

(a) *Refinement boxes | Steady | Side view*

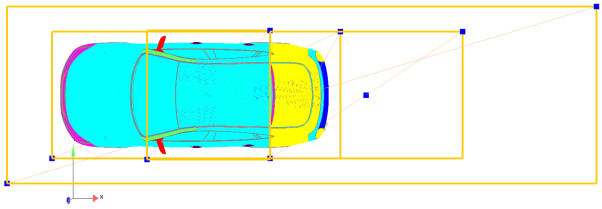

(b) *Refinement boxes | Steady | Top view*

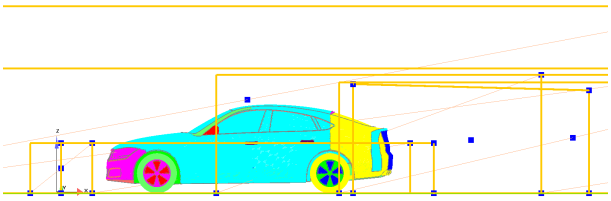

(c) *Refinement boxes | Unsteady | Side view*

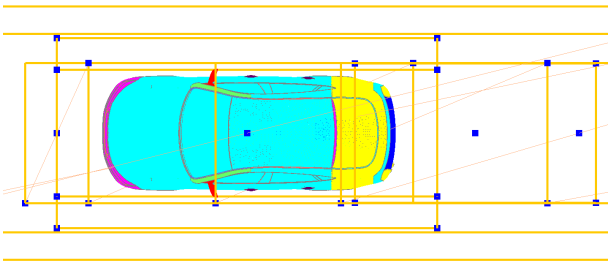

(d) *Refinement boxes | Unsteady | Top view*

Figure 3.3: *Refinement boxes*

The resulting mesh consists of $50E6$ cells for the steady method and $200E6$ cells for unsteady and steady enhanced wall treatment methods. Illustrations of the two different meshes used in this work can be seen in figure 3.4. The two meshes will be called steady mesh or 50M, and unsteady mesh or 200M.

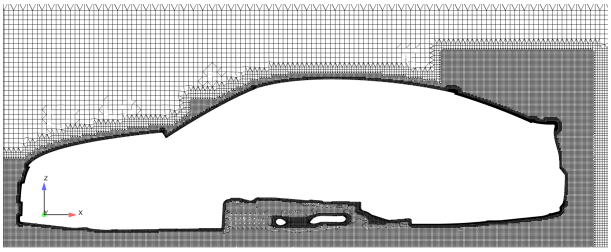

(a) *Mesh Y_0 plane | Steady (50M)*

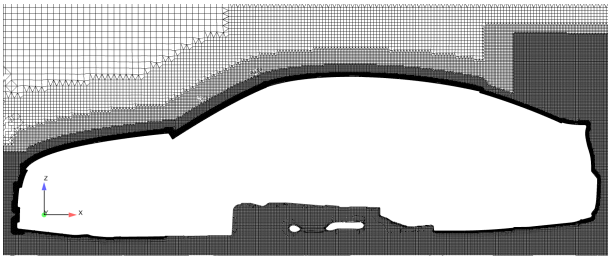

(b) *Mesh Y_0 plane | Unsteady (200M)*

Figure 3.4: *Mesh | Y_0 plane*

3.3 Solving

Solving is the act of calculating the flow field of the domain using the theory briefly described in chapter 2. The main difference between the three procedures is that only one takes time into account. The steady solution is a time averaged flow that can't account for the natural fluctuating behaviour of turbulent flow. This is what leads to a vast difference in need of computational power. It is important to note that all simulations and experiments consist of full car, moving ground, and rotating wheels with moving reference frame used between the wheel spokes. Furthermore all numerical results are from a free stream velocity of $27.78m/s$, $100km/h$.

The three different solving methods are denoted steady, SS, steady enhanced wall treatment, SS-EWT, and unsteady, US. Solutions from the three methods are post-processed in the same way in order to enable qualitative comparison since it is the main tasks of this work.

Table 3.1 summarises the different methods used and the solving time required. The method denoted US interpol. is the same as the US method except that after the first set of US simulations were performed, the following simulations used the interpolated results to significantly speed up the solving time.

Table 3.1: Summary of methods used

Method	Solving method	Iterations	Flow time	Mesh size	CPU time
SS	Real. $k-\epsilon$ - SWT	2000	NaN	$50E6$	2000 core hours
SS-EWT	Real. $k-\epsilon$ - EWT	3000	NaN	$200E6$	4000 core hours
US	$SA-DDES$	5 sub. it.	$8s$	$200E6$	160000 core hours
US interpol.	$SA-DDES$	5 sub. it.	$6s$	$200E6$	120000 core hours

3.3.1 Steady

The steady solution is obtained using realisable the $k-\epsilon$ turbulence model, which is very common in industry. The solution is robust and converges well within 2000 iterations. Some configurations in this work will be using the same mesh as the unsteady method with the steady solver and enhanced wall treatment, EWT, which requires 3000 iterations to reach a converged solution. The computational time required is 2000 core hours for the SS method and 4000 core hours for the SS-EWT method. Further in depth description of the steady procedure is found in [7].

3.3.2 Unsteady

The unsteady solution consists of a delayed detached eddy simulation, DDES, which is initialised using a steady solution. One flow pass, two seconds, is used to stabilise the initial solution using a time-step of 5E-4 before data-averaging with a smaller time-step of 2E-4s, using five sub-iterations per time-step. Two to four flow passes is required to reach a converged solution in the meaning of a fluctuation of less then a count during the last flow pass for the running average of the drag, front lift, and rear lift. The computational time required is 160000 core hours for an total of four flow passes, or a total flow time of $8s$. Figure 3.5 illustrates the drag coefficient versus time in a running average, the case has been data averaged after 1 second since it is based on a previous unsteady case using interpolation. This was one of the early cases and has been run to long as is seen in the figure, according to the recomendations of [8], this simulation should have been stopped soon after 6 seconds of flow time. The following simulations are based on interpolated results from the baseline simulations, allowing for a reduction in simulated flow time. The interpolated simulations required 120000 core hours for an total of three flow passes. Further in depth description of the unsteady procedure is found in [8].

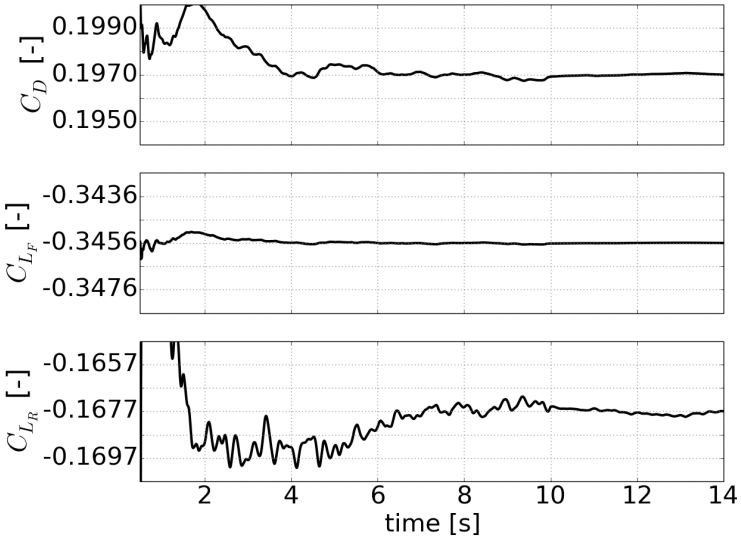

Figure 3.5: *C_d vs T | Running average | Unsteady*

To illustrate the performance of the SA-DDES method according to the guidelines in [9], DES limiter, viscosity ratio, and resolved and modelled turbulent kinetic energy are shown in figure 3.6. It is evident that the DES limiter functions as intended, seen in figures 3.6a and 3.6b, by only using the RANS mode, $f_d = 0$, near the car and ground and transitioning quickly to LES mode, $f_d = 1$. The turbulent viscosity ratio illustrated in figures 3.6c and 3.6d show that areas such as underbody, wheel houses and wake are the areas that exhibit high

turbulent viscosity ratio. The level of resolved and modelled turbulent kinetic energy, illustrated in figures 3.6e, 3.6f, 3.6g and 3.6h, show that the same areas indicated by a high turbulent viscosity ratio are modelled instead of resolved. In the whole flow field, more than than 80% of the stresses in the turbulent kinetic energy are resolved, as recommended by the guidelines in [9].

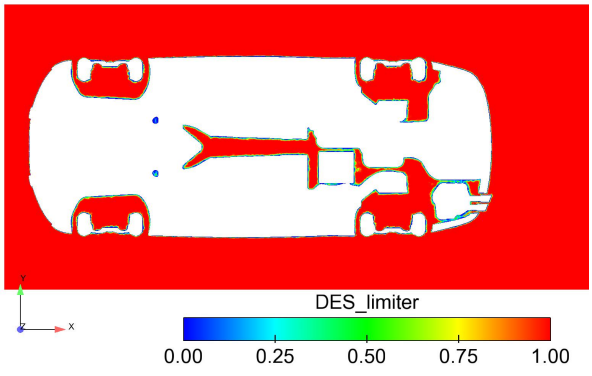

(a) *DES limiter | Z plane wheel center height*

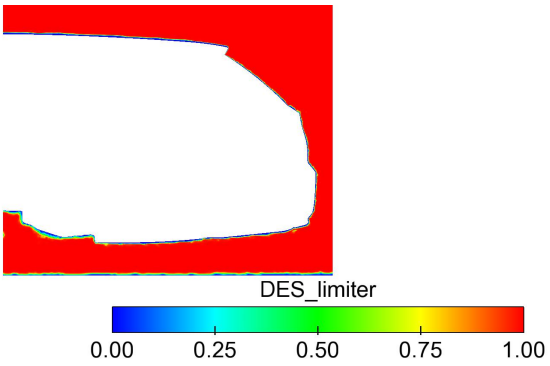

(b) *DES limiter | Symmetry plane*

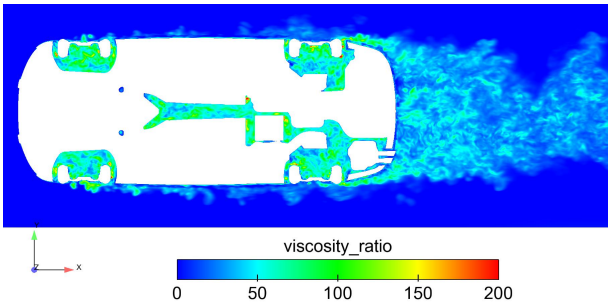

(c) *Turbulent viscosity ratio | Z plane wheel center height*

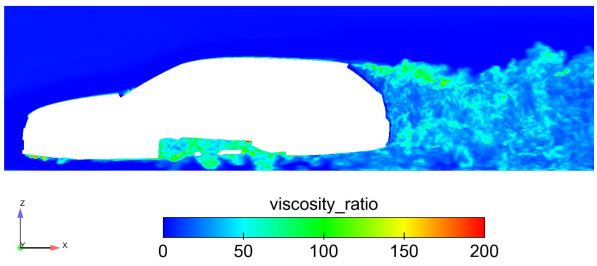

(d) *Turbulent viscosity ratio | Symmetry plane*

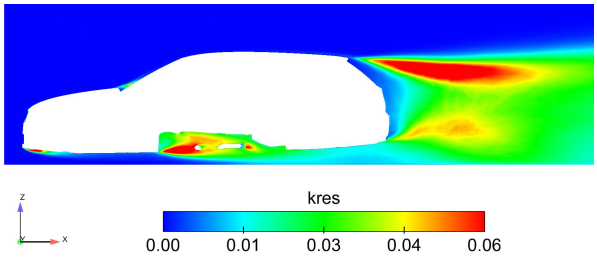

(e) *Resolved turbulent kinetic energy | Symmetry plane*

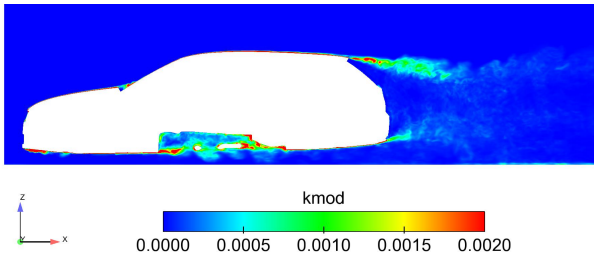

(f) *Modelled turbulent kinetic energy | Symmetry plane*

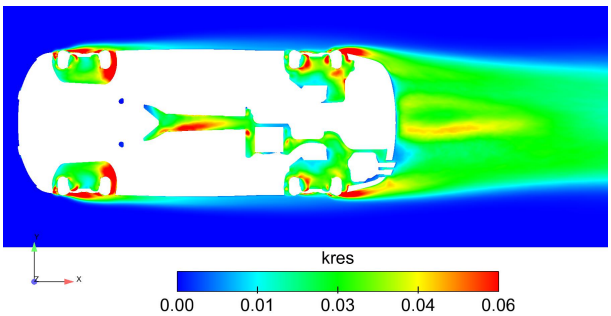

(g) *Resolved turbulent kinetic energy | Z plane wheel center height*

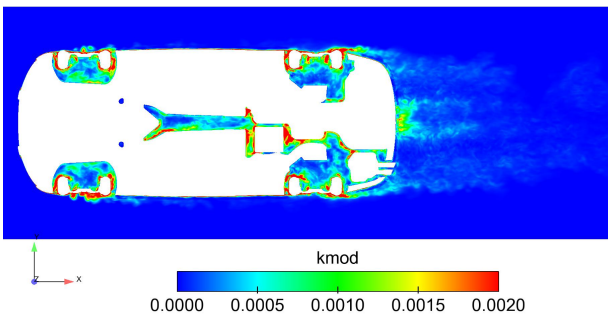

(h) *Modelled turbulent kinetic energy | Z plane wheel center height*

Figure 3.6: *SA-DDES Performance | Baseline | Squareback*

3.4 Experimental data

The experimental data denoted PVT consists of full scale testing in the Volvo Wind Tunnel, using ground simulation system, with correction for blockage. The data denoted PVT UC is the uncorrected data from PVT. The data is provided by Ford of Europe, whom have built a full scale model of the DrivAer model. Further details regarding the Volvo Wind Tunnel and its recently upgraded test section are found in [10].

There are two differences between the DrivAer model and the fullscale model used in PVT. The PVT model has suspension components, which was not included in the DrivAer model at the time of this work, and slightly different angles on the wheel spokes and tires, which is illustrated in figure 3.7. The affect of these geometrical differences is discussed in section 5.2.

(a) *DrivAer model wheels* (b) *PVT model wheels*

Figure 3.7: *Geometrical differences | Wheels PVT*

The data denoted TUM consists of 40% scale testing in the TU München Wind Tunnel, using moving ground and stings to mount the model and wheels, seen in figure 3.8a. Since there are two different data sets published from TUM, one a SAE paper and one a ASME paper, they are denoted TUM SAE [1] and TUM ASME [2].

Some surface pressure and wake measurements have been concluded at TU Berlin, TUB [4] [3]. Results from these papers are generated without moving ground but with some boundary layer control, see figure 3.8b, and the results are only used for visual comparison. The affect of these geometrical differences is discussed in section 5.2.

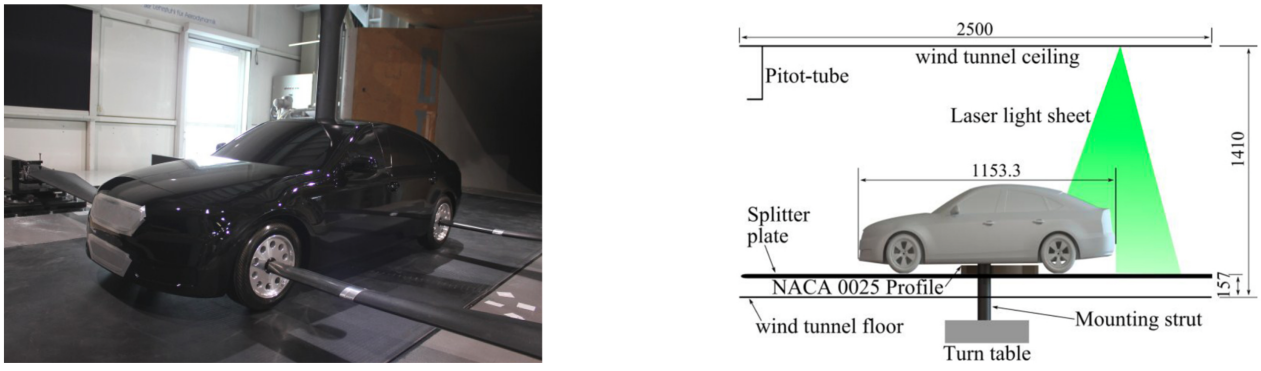

(a) *TU München | Setup* (b) *TU Berlin | Setup*

Figure 3.8: *Geometrical differences and setups | Scale models*

4 Results

The results are divided according to vehicle model and underbody configuration, within each configuration a comparison between the three different numerical methods is presented and a comparison to experimental data. All unsteady results are time averaged, and all numerical results are based on converged solutions, which is discussed in section 3.3.

Some planes used in the figures are the symmetry line plane or Y_0 plane, which is the $Y = 0m$ plane, centre line of the vehicle. The plane called Z plane is the $Z = 0.824m$ plane, which is roughly in the same height as the door handles, and finally the plane called X plane is the plane $0.1m$ behind the rear end of the vehicle.

To confirm that the solution is mesh dependant and not as much wall treatment dependant, both wall treatments were used on both the meshes for the baseline and smooth underbody configurations. The results show that the wall treatment has almost no impact on the forces and flow field. Therefore the methods denoted SS or SS-SWT:50M, SS-EWT or SS-EWT:200M, and US or US:200M are those methods that will be discussed and presented. The methods denoted SS-EWT:50M and SS-SWT:200M, which stands for 50 million cells steady - standard wall treatment and 200 million cells steady - enhanced wall treatment, are shown in the presentation of drag forces but are not discussed or illustrated since their purpose is only to prove that the mesh has largest influence on the difference between the methods used.

4.1 Baseline

Since several sources of experimental data is used, a compilation of all numerical and experimental data is used to provide an overview of the spread, seen in figure 4.1. The SS and US methods correlate well with the TUM SAE, TUM ASME, and PVT UC results for the fastback model, with an maximum error of 4 counts. The SS-EWT method correlates better with the PVT data with an drag over prediction of 6 counts.

Similar behaviour is observed for the notchback model but with a slightly larger spread. The US method correlates well with the TUM SAE, TUM ASME and PVT UC data, with an over prediction of 1 to 7 counts. The SS-EWT method correlates very good with the PVT data with an error of 3 counts. The SS method correlates best with the PVT UC data with an under prediction of 5 counts.

Furthermore the squareback model has good correlation between the SS, SS-EWT methods and the PVT data with an under prediction of 7 counts. The US method correlates well with both data sets from TUM with an under prediction of 1 to 6 counts while it correlates slightly worse with the PVT UC data with an over prediction of 8 counts.

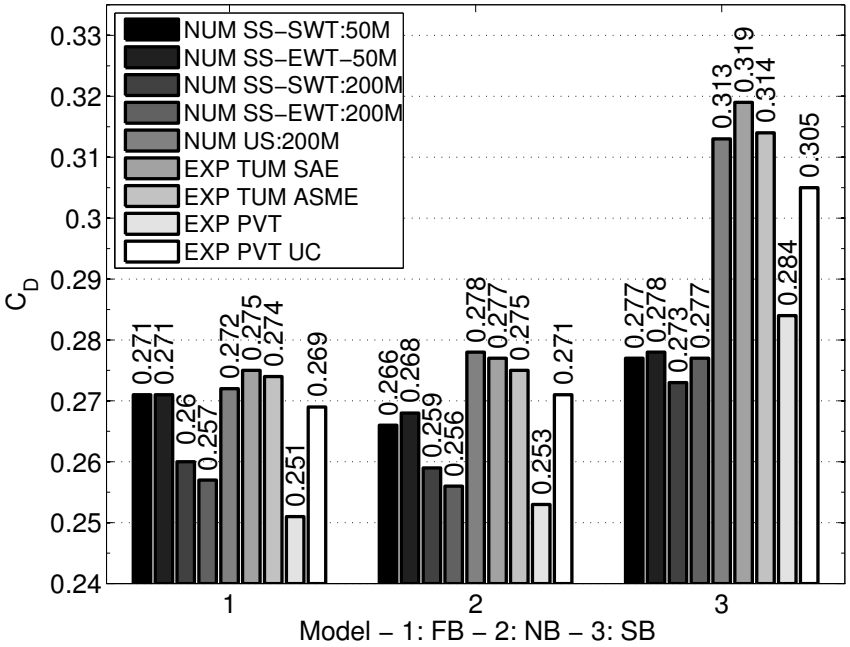

Figure 4.1: C_D | *Data spread* | *Baseline*

The PVT data is regarded as the most reliable experimental data in this work it thus used for closer comparison of the three numerical methods, seen in figure 4.2. Both the US and SS methods over predicts drag for the fastback and notchback models with 13 to 25 counts while the SS-EWT method correlates very good with an drag over prediction of 3 to 6 counts. Continuing to the squareback model a different behaviour is observed, the US method over predicts drag with 29 counts while the SS and SS-EWT methods under predicts drag with 7 counts. Furthermore a compilation of the results compared to PVT UC, meaning the uncorrected PVT results, can be seen in figure 4.3.

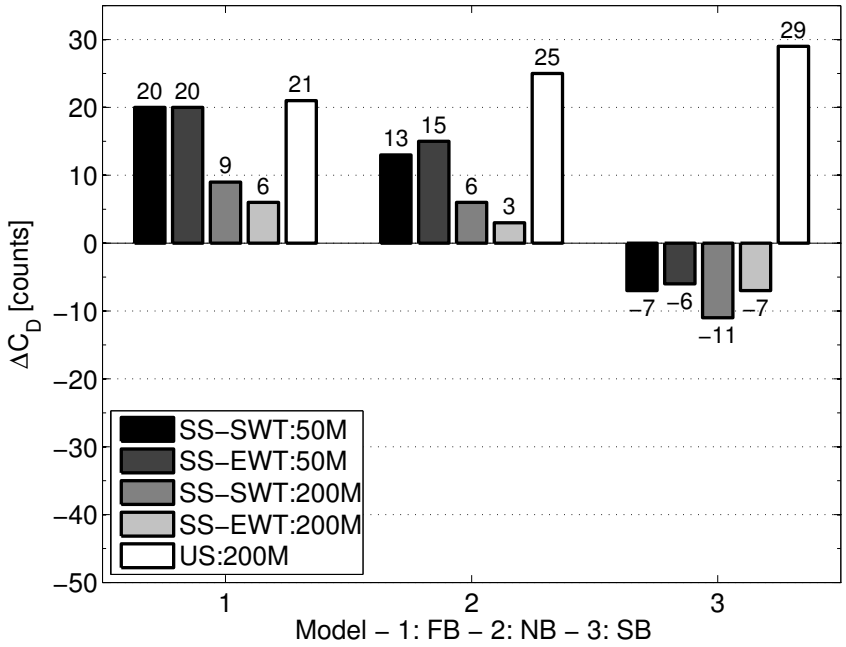

Figure 4.2: ΔC_D | *Baseline* | *REF Exp PVT*

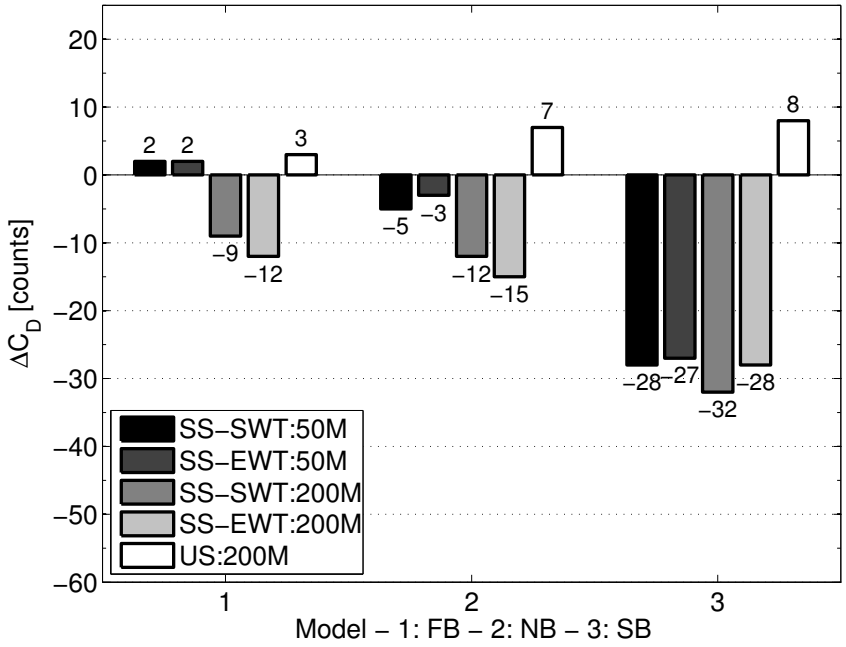

Figure 4.3: ΔC_D | *Baseline* | *REF Exp PVT UC*

4.1.1 Baseline | Fastback

There are several reasons for the difference in drag between the different methods. The base wake pressure is an important factor to investigate due to its great impact on the overall drag of the vehicle. The SS method shows signs of reattachment close to the tail lights while both the SS-EWT and US methods show a clearer separation, as seen in figure 4.4. The US method seems to slightly recirculate to the lower right hand side of the base wake, leading to increased drag, in an quite asymmetrical manner, which could be caused by the asymmetrical underbody. The SS-EWT method has the cleanest separation and also the least drag over prediction.

Velocity streamlines along the symmetry line are used to further investigate the wake behaviour, see figure 4.4. It is evident that strong recirculation occurs for the SS method in the top of the wake. The US method shows recirculation in both the top and bottom part of the wake while the SS-EWT method indicates less recirculation.

The Z plane velocity streamlines in figure B.1, show that the SS method generates a significantly narrower wake in this plane when compared to the SS-EWT and US methods. The X plane total pressure distribution in the same figure indicates that the SS and SS-EWT methods generate a similar pattern in the wake while the US method exhibits a more compact pattern in the wake which looks more realistic when compared to the more sprawling behaviour exhibited by the SS and SS-EWT methods.

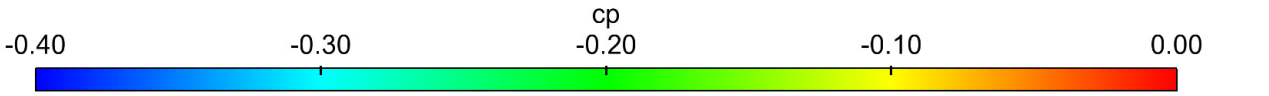

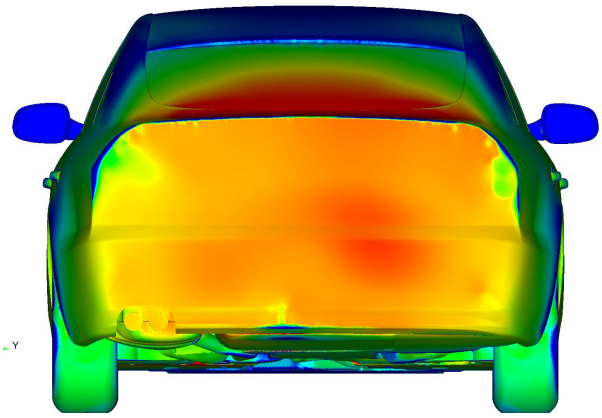

(a) C_p | *Steady*

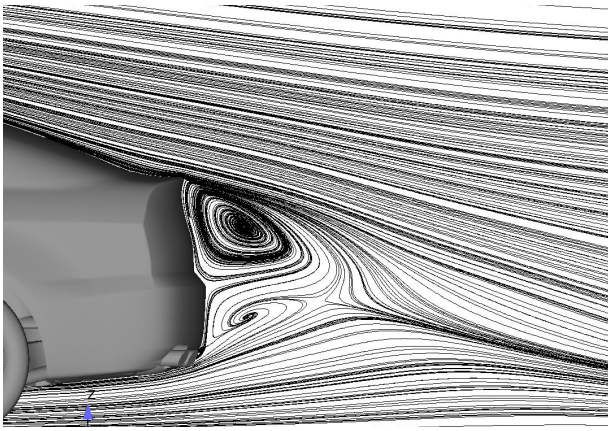

(b) *Velocity streamlines* | *Steady*

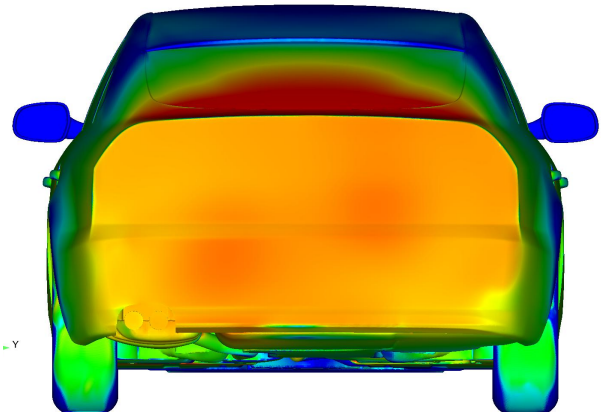

(c) C_p | *Steady EWT*

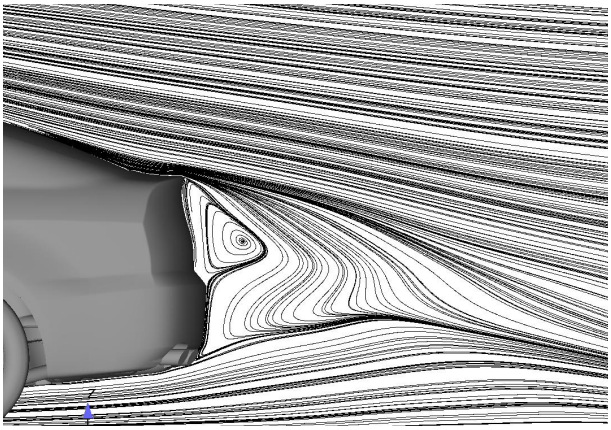

(d) *Velocity streamlines* | *Steady EWT*

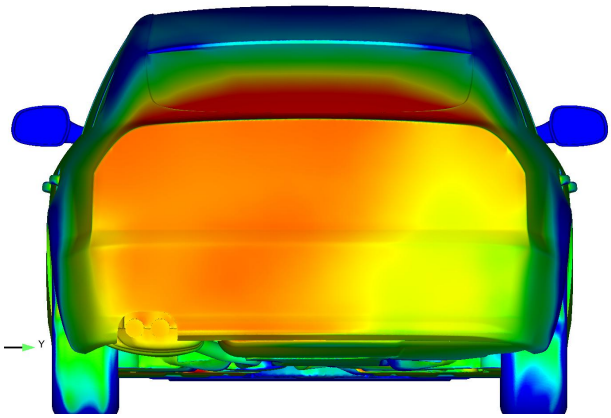

(e) C_p | *Unsteady*

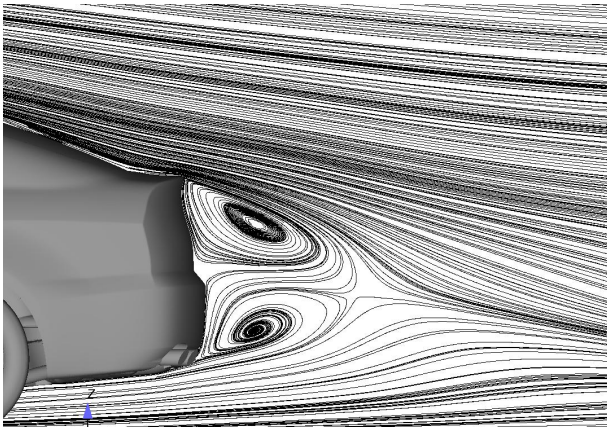

(f) *Velocity streamlines* | *Unsteady*

Figure 4.4: C_p *Rear view & Velocity streamlines* Y_0 | *Baseline* | *Fastback*

To further investigate the differences between the three numerical methods and compare them to experimental data, surface pressure is illustrated along the symmetry line of the car, as seen in figure 4.5. The experimental data from TUM SAE is obtained through built in pressure probes in a 40% scale model, further information can be found in [1]. The US and SS-EWT have very similar behaviour, and seem to correlate slightly better to the experimental data than the SS method. Areas such as the plenum and beginning of the roof seem to be where the SS method does not correlate as well as the two other methods used. A noticeable difference can also be observed in the front part of the engine under shield and beginning of the hood. These are areas where the SS method exhibits a higher pressure than the two other methods used.

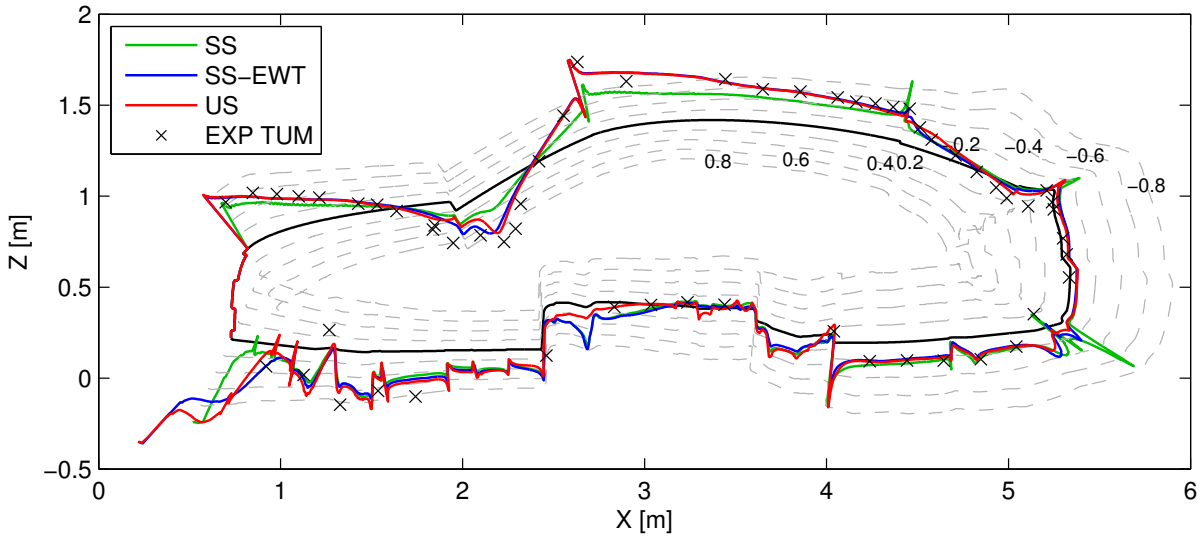

Figure 4.5: C_p *vs* X | *Symmetry line* | *Baseline* | *Fastback*

4.1.2 Baseline | Notchback

The notchback has very similar geometry as the fastback and thus slightly similar flow field. The same findings as for the fastback can be observed when investigating the base wake pressure, see figure 4.6. The SS method shows recirculation close to the tail lights while the US method show a slight recirculation along the lower right hand side of the base wake. In both cases this can indicate an increase in drag when compared to the SS-EWT method which shows a cleaner separation. It can also be seen that the US method has a delayed separation on the rear window compared to the SS and SS-EWT methods.

Further investigation of the wake is illustrated in figure 4.6, using velocity streamlines along the symmetry of the vehicle. The US method generates recirculation for the bottom part of the wake, with the bottom part being the strongest and quite close to the vehicle. The SS method shows a strong recirculation in the top part of the wake, similar to the SS-EWT method but in a larger extent.

The X plane total pressure distribution and Z plane velocity streamlines, see figure B.2 looks very similar as for the fastback model. The SS-EWT and US methods have a similar behaviour, except for the US methods recirculation occurring closer to the vehicle and a more compact and realistic total pressure distribution. Furthermore the SS method generates a narrower wake when compared to the two other methods used, and the vortices appear less developed.

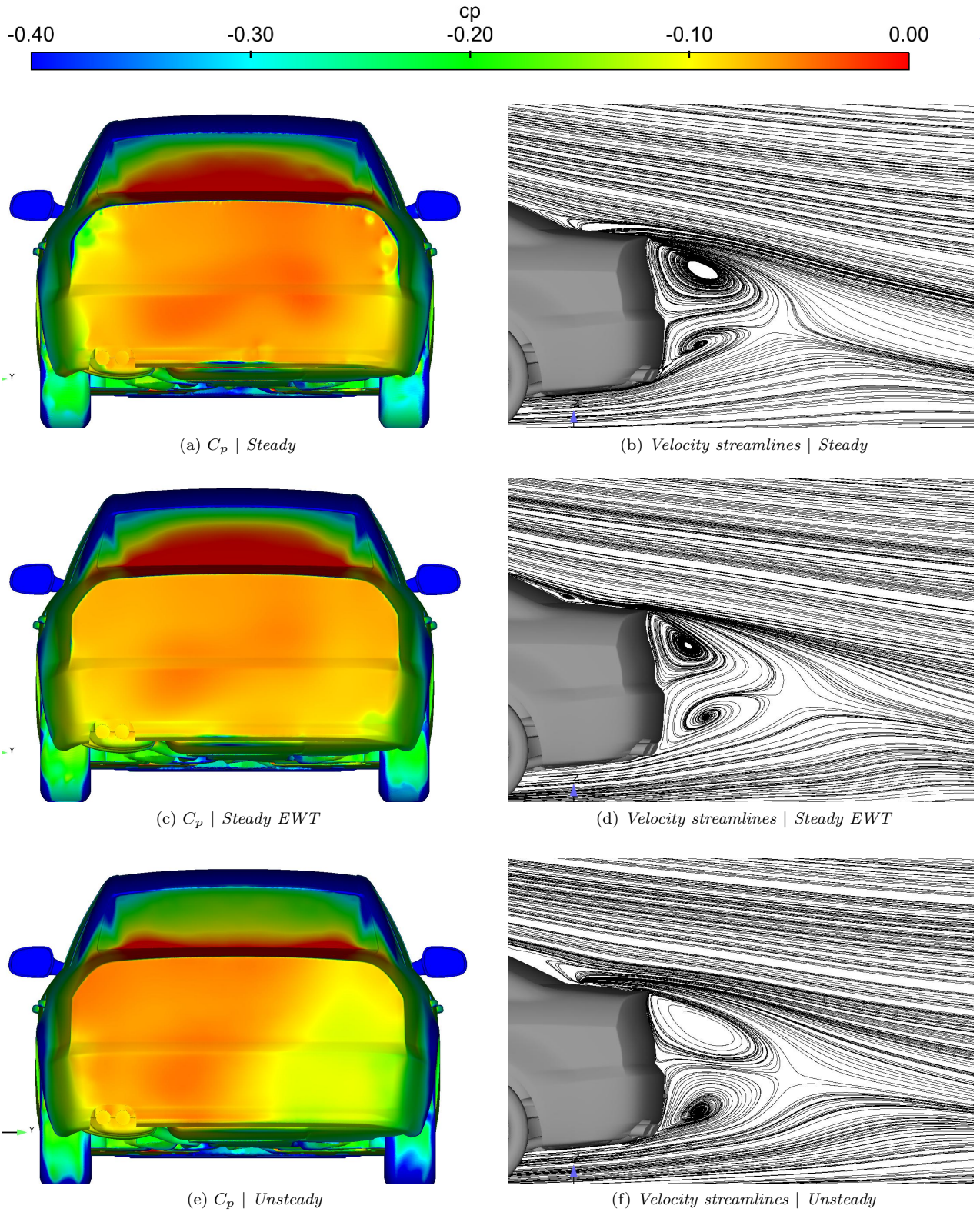

(a) C_p | *Steady*

(b) *Velocity streamlines* | *Steady*

(c) C_p | *Steady EWT*

(d) *Velocity streamlines* | *Steady EWT*

(e) C_p | *Unsteady*

(f) *Velocity streamlines* | *Unsteady*

Figure 4.6: C_p *Rear view & Velocity streamlines* Y_0 | *Baseline* | *Notchback*

Comparison of symmetry line pressure distribution, figure 4.7, leads to similar observations as for the fastback model. The SS-EWT and US methods have similar pressure distribution and correlate better with the experimental data. The SS method once again exhibits a higher pressure in the front part of the engine under shield and have a slightly higher pressure over the roof, which could generate differences in lift forces.

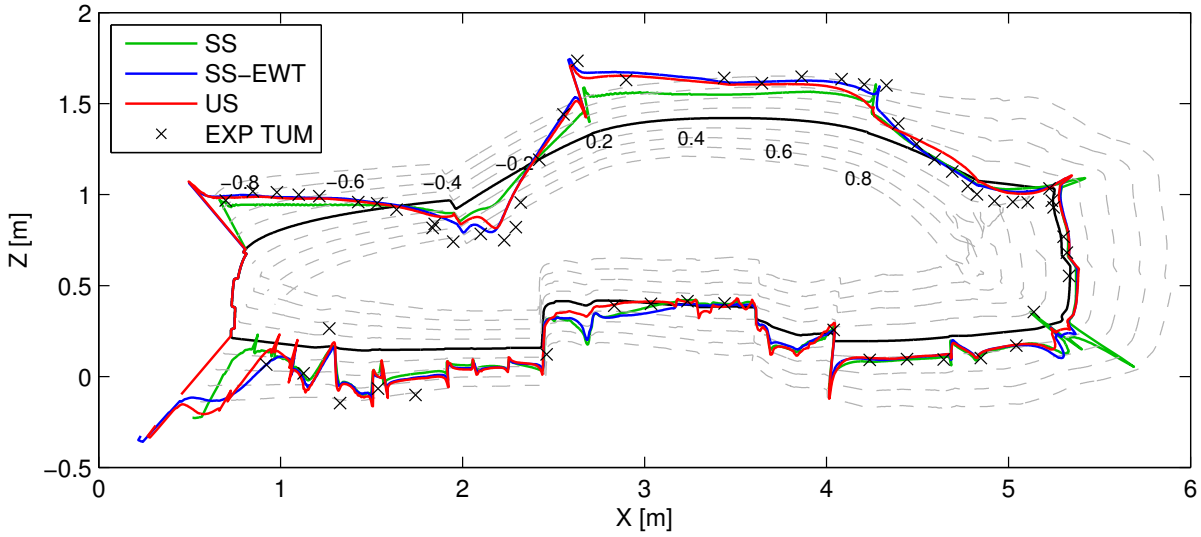

Figure 4.7: C_p *vs* X | *Symmetry line* | *Baseline* | *Notchback*

4.1.3 Baseline | Squareback

The geometry of the squareback differs quite allot from the two other vehicle models, and also the flow field of the three different numerical methods. The data in figure 4.2 show that the US method over predicts the drag while the SS and SS-EWT methods under predicts drag, when compared to PVT data. The same behaviour can be seen in the base wake pressure distribution, figure 4.8, where the US method generates roughly 100 counts lower pressure coefficient in the majority of the lower area of the base wake. The US and SS-EWT methods indicate descent separation while the SS method indicates recirculation along the tail lights and bumper.

Investigation of velocity streamlines along the symmetry of the wake, see figure 4.8, further strengthens the previous findings. The US method has only a small part of recirculation in the bottom part of the wake. Both the SS and SS-EWT methods indicate recirculation in the bottom part of the wake and also in the top part a bit behind the vehicle. The vortices seem further developed in the SS-EWT method compared to the SS method, even though the pattern is very similar.

The total pressure distribution in figure B.3 indicate that the US method generates a more compact and realistic wake and while the SS and SS-EWT methods spreads out more. The two latter methods have very similar patterns which can also be seen in the Z plane velocity streamlines in the same figure. The SS and SS-EWT methods exhibits similar pattern with strong vortices on both sides of the wake. The US method exhibits a flow biased to the right ride of the vehicle seen from the rear, and is closer to the vehicle than the two other methods. This is possible one reason to the lower pressure regions in the base wake.

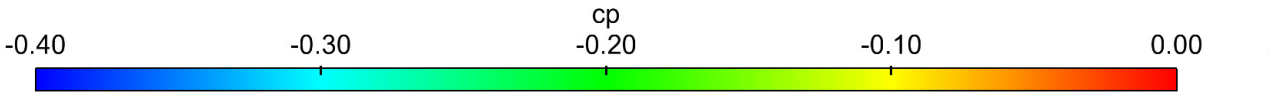

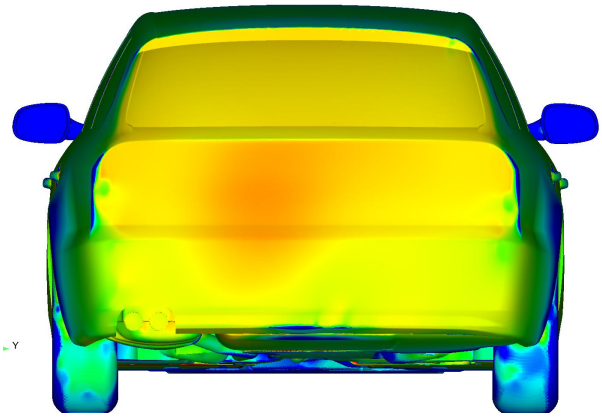

(a) C_p | *Steady*

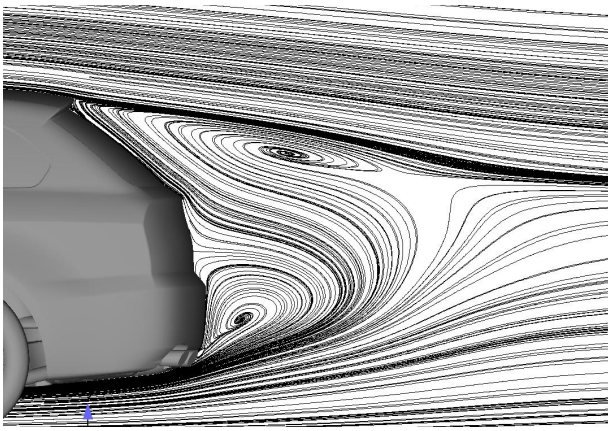

(b) *Velocity streamlines* | *Steady*

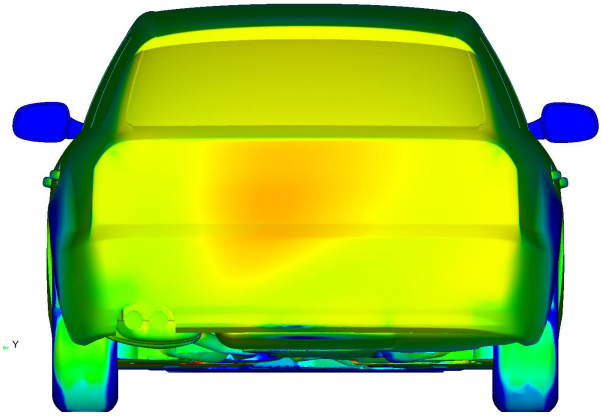

(c) C_p | *Steady EWT*

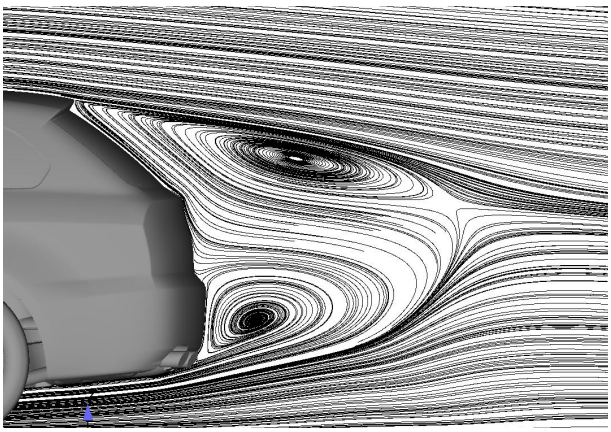

(d) *Velocity streamlines* | *Steady EWT*

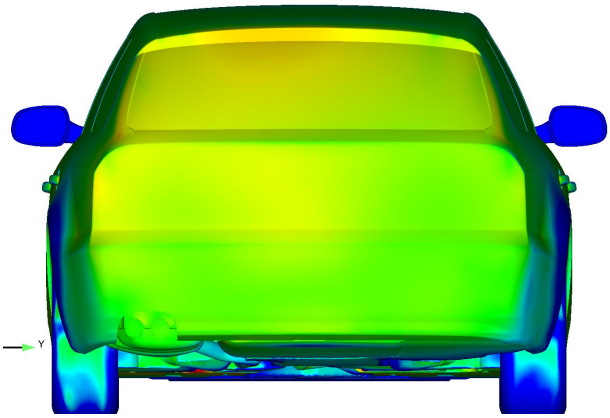

(e) C_p | *Unsteady*

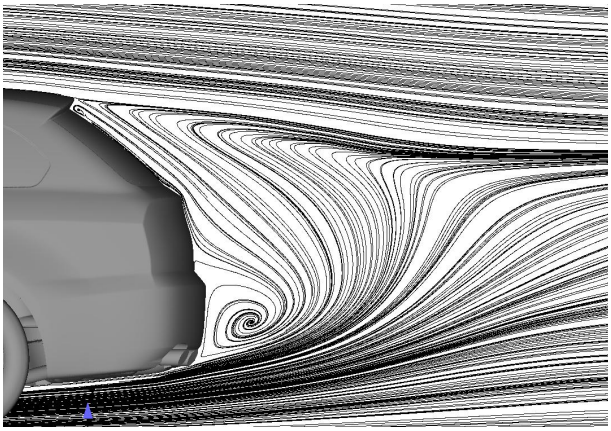

(f) *Velocity streamlines* | *Unsteady*

Figure 4.8: C_p *Rear view & Velocity streamlines* Y_0 | *Baseline* | *Squareback*

The symmetry line pressure distribution, figure 4.9, show the same behaviour as the other two models. The US and SS-EWT methods have very similar pressure distribution and correlate well with the TUM data, while the SS method exhibits a higher pressure in the front part of the engine under shield. Furthermore the SS method predicts higher pressure on the front part of the roof and lower pressure near the plenum.

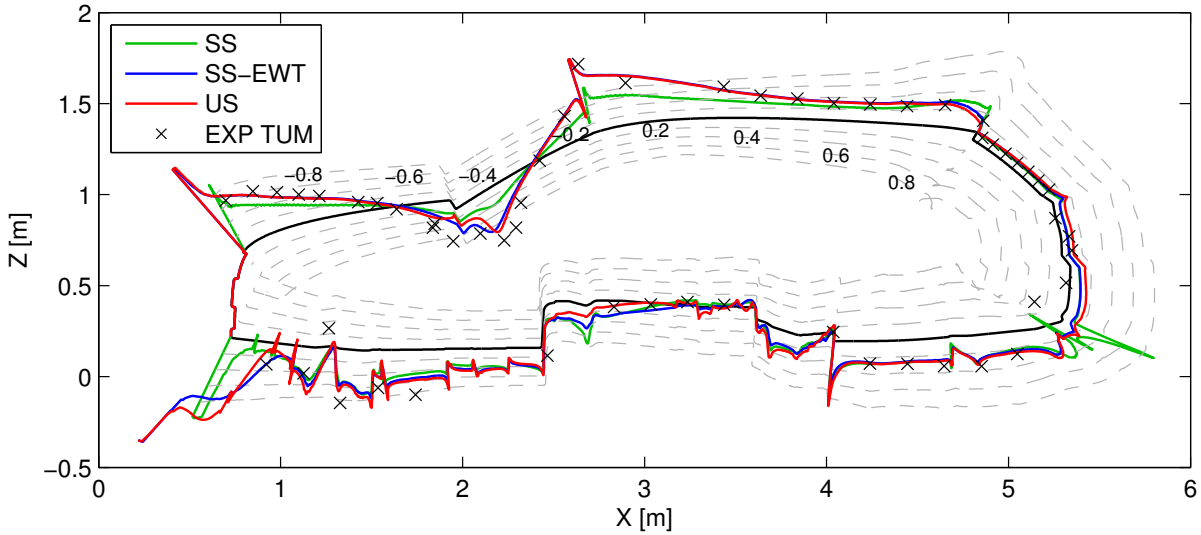

Figure 4.9: C_p *vs* X | *Symmetry line* | *Baseline* | *Squareback*

4.2 Smooth underbody

The smooth underbody configurations have some spread between the different numerical methods, see figure 4.10. For the fastback model the SS and SS-EWT methods correlates best with the PVT data with a drag under prediction of 14 counts. The US method correlates fairly well with all experimental data and under predicts drag with 8 to 12 counts when compared to the TUM SAE, TUM ASME and PVT UC data. When compared to the PVT data the US method over predicts drag with 7 counts.

Very similar behaviour is observed for the notchback model, the SS and SS-EWT methods has poor correlation and is closest to the PVT data with an drag under prediction of 16 to 19 counts. The US method under predicts drag with 3 counts when compared to the TUM SAE and PVT UC data, and The over predicts drag with 12 counts when compared to the PVT data.

Finally for the squareback model the SS and SS-EWT methods greatly under predicts drag with 28 to 36 counts compared to PVT data. Furthermore the US method correlates well with the TUM SAE, TUM ASME and PVT UC data with an drag over prediction of 0 to 4 counts.

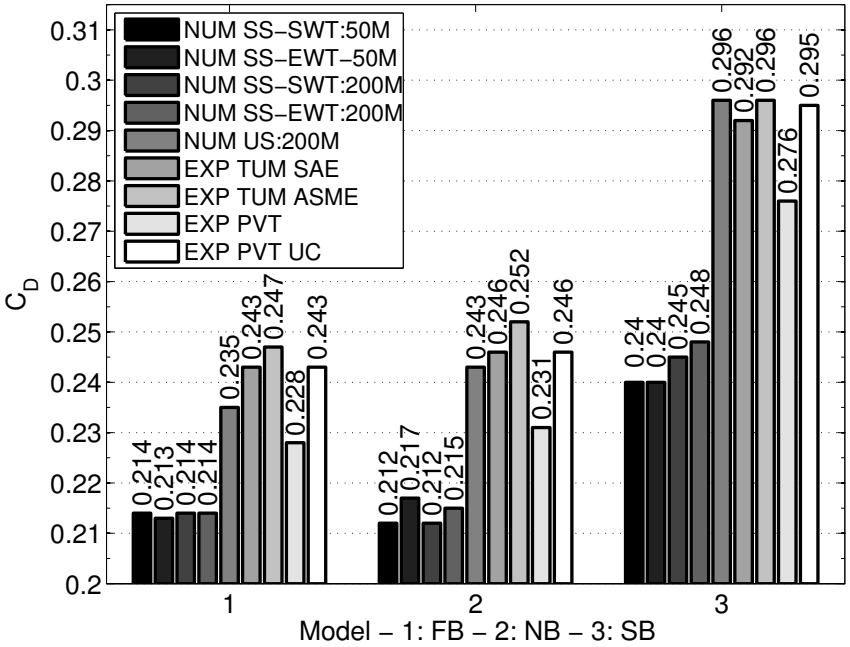

Figure 4.10: C_D | *Data spread* | *Smooth underbody*

There are several recent papers with numerical results for the fastback and squareback model with smooth underbody, a compilation of them can be seen in figure 4.11. The data denoted UNC & UMAN is published by UNC Charlotte Motorsports Engineering [6] and University of Manchester [5]. This data consists of recent numerical simulations using steady and unsteady methods. For the fastback model a consistent over prediction of drag is observed for all results from UNC and UMAN. For the squareback model a different behaviour can be observed, a drag over prediction is observed for the UMAN US results while a drag under prediction is observed for the UNC & UMAN SS results. For the latter mentioned methods there are some data points with good correlation with the PVT results.

The numerical methods used in this work have good performance when compared to the methods used in the UNC and UMAN results, and the total spread of all the fastback model results is 54 drag counts and 73 drag counts for the squareback model.

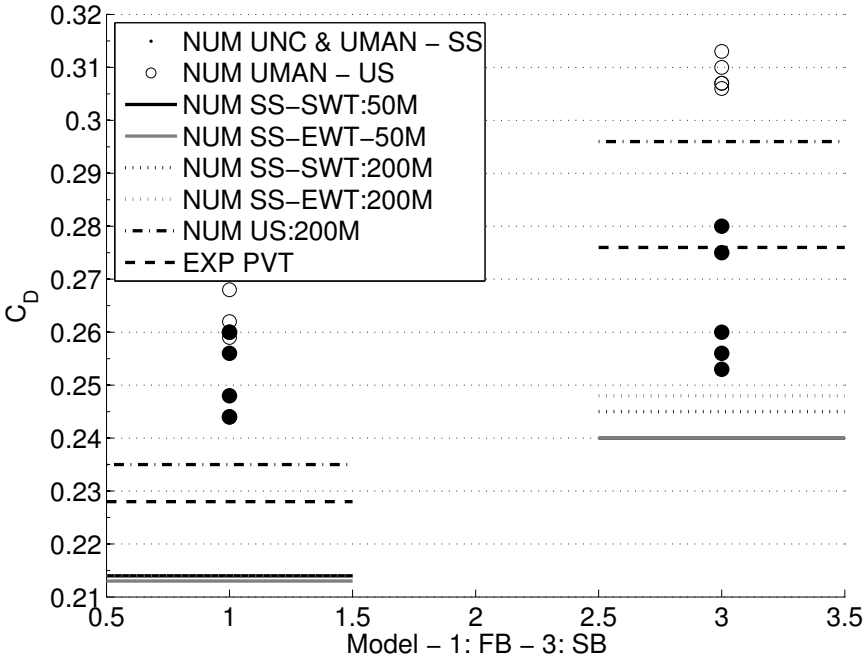

Figure 4.11: C_D | *Numerical data spread* | *Smooth underbody*

The behaviour of the numerical methods are similar for all three vehicle models when investigating the smooth underbody configurations. The US method over predicts the drag while both the SS and SS-EWT methods under predict the drag, see figure 4.12. The fastback and notchback model have similar results with the US method over predicting drag with 7 to 12 counts while the SS and SS-EWT methods under predict drag with 14 to 19 counts. The squareback has a larger error with the US method over predicting drag with 20 counts and the SS and SS-EWT methods under predicting drag with 28 to 36 counts. Furthermore a compilation of the results compared to PVT UC, meaning the uncorrected PVT results, can be seen in figure 4.13.

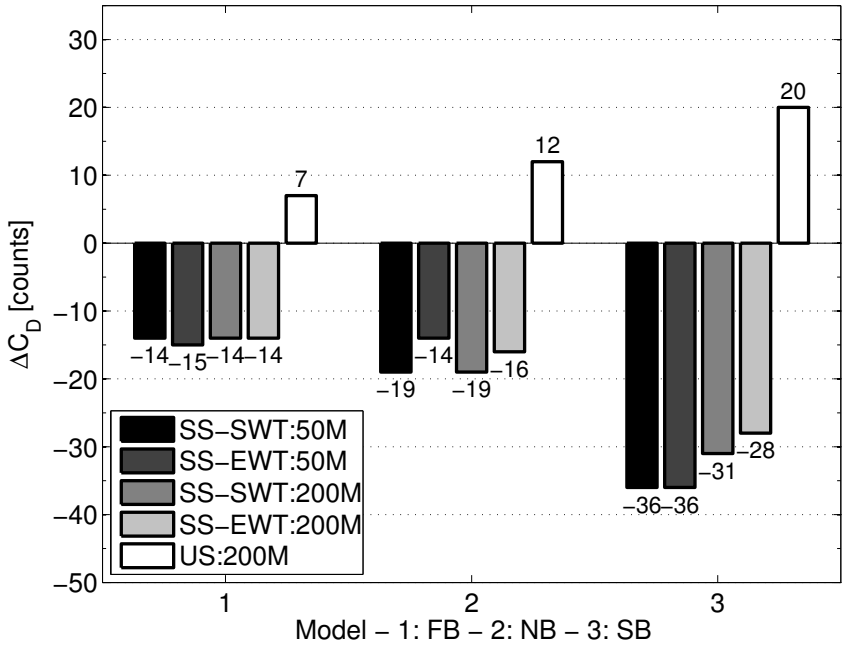

Figure 4.12: ΔC_D | *Smooth underbody* | *REF Exp PVT*

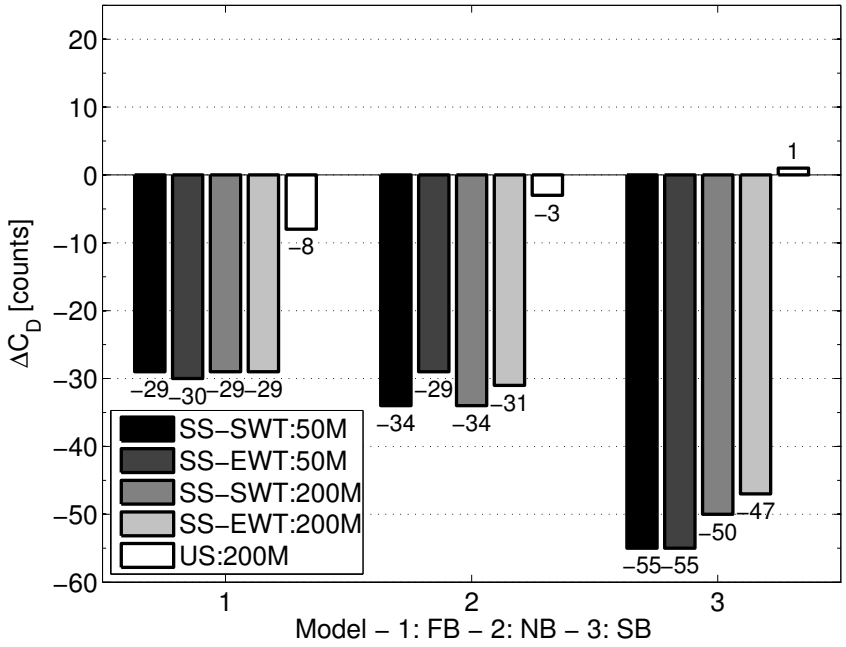

Figure 4.13: ΔC_D | *Smooth underbody* | *REF Exp PVT UC*

To further investigate the differences between the three methods used, the difference between configurations is used in figure 4.14. The difference between the baseline and smooth underbody configuration is investigated with the PVT data set as reference. The SS method exhibits the greatest error with an under prediction of 29 to 34 drag counts for all three vehicle models. The SS-EWT method has a slightly smaller error with an drag under prediction of 19 to 21 counts for the different models. Finally the US method has the smallest error of 9 to 14 drag counts. This is a good index of the correlation since comparing absolute values is not always accurate due to differences in the physical and virtual wind tunnel geometry, and differences between the models.

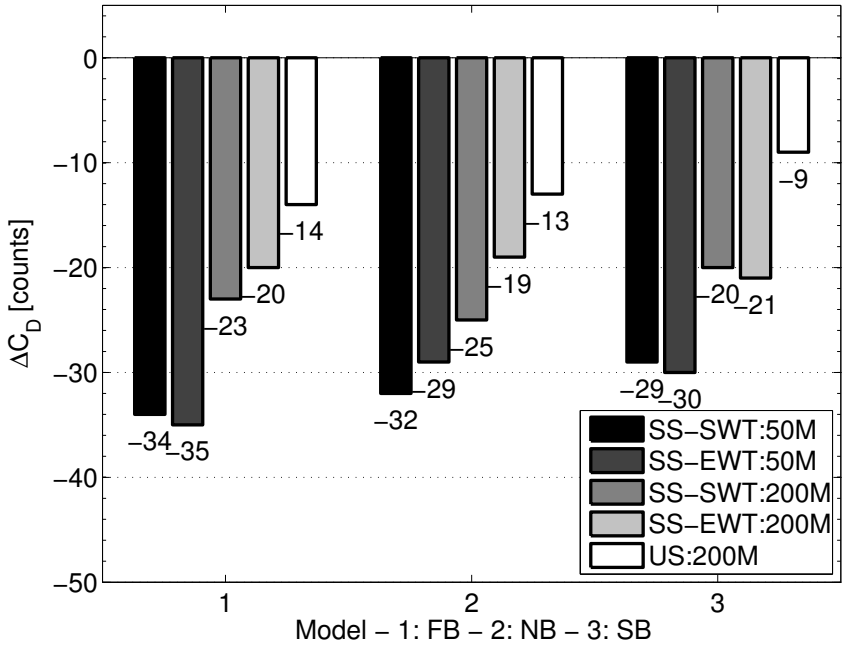

Figure 4.14: ΔC_D | *Influence of Smooth underbody* | *REF Exp PVT Baseline*

4.2.1 Smooth underbody | Fastback

Figure 4.12 shows an over prediction of drag for the US method and under prediction of drag for the SS and SS-EWT methods. Investigating the base wake pressure distribution in figure 4.15 further strengthens these findings. The SS and SS-EWT have very similar pressure distribution except for around the bumper where the SS method exhibits a more attached flow. The pressure distribution of the US method is quite different where it indicates a symmetrical recirculation on the sides of the base wake, decreasing the surface pressure and thus increasing the drag compared to the other two methods. Similar behaviour can be seen in pressure measurements from scale model wind tunnel testing at TUB [3].

Investigation of the symmetry line wake in figure 4.15 indicates a strong top and bottom recirculation close to the vehicle in the SS method while the SS-EWT method tends to have a stronger recirculation in the bottom compared to the top. Contrary to the SS-EWT method, the US method tends to recirculate in the top part of the wake.

The X plane total pressure distribution and Z plane velocity streamlines in figure B.4 show that the SS and SS-EWT methods generate a very similar sprawling behaviour in the wake while the US method has a more compact and realistic wake. Furthermore the US method recirculates closer to the vehicle with further developed vortices than the two other methods used, thus generating the low pressure zones as seen in figure 4.15e. It should also be noted that the SS method has a narrower pattern than the two other methods in the Z plane velocity streamlines.

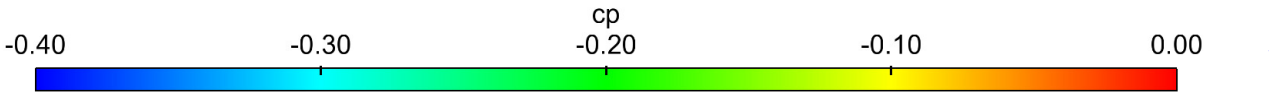

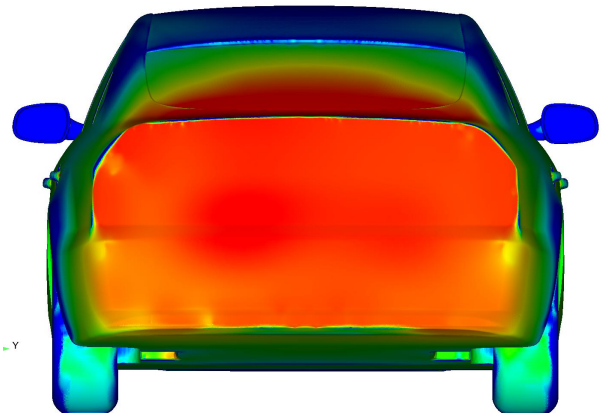

(a) C_p | *Steady*

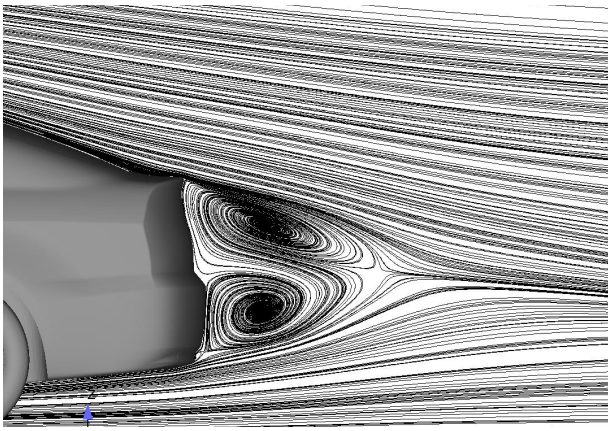

(b) *Velocity streamlines* | *Steady*

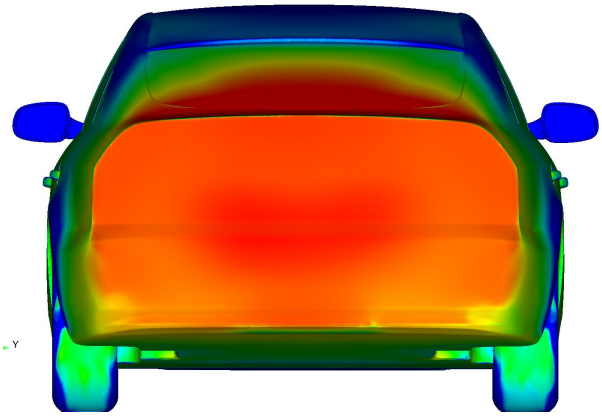

(c) C_p | *Steady EWT*

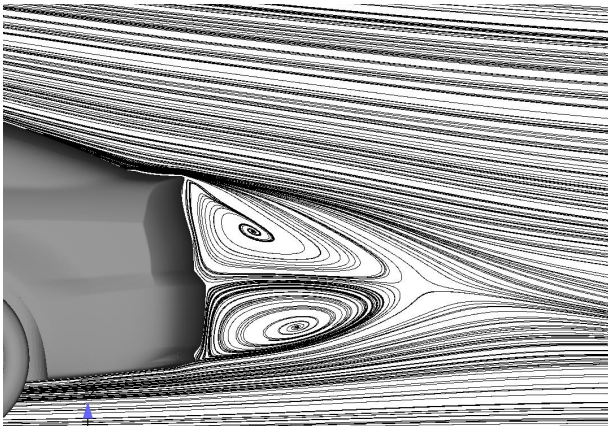

(d) *Velocity streamlines* | *Steady EWT*

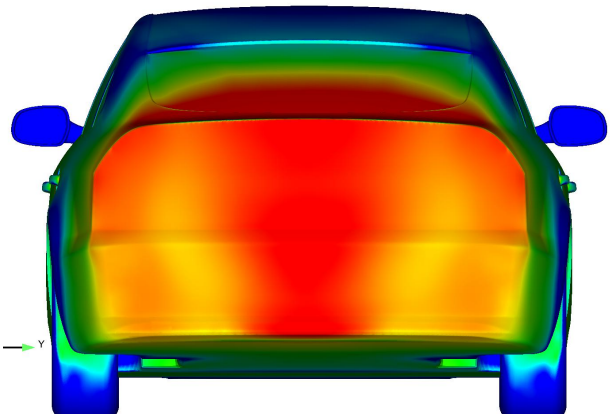

(e) C_p | *Unsteady*

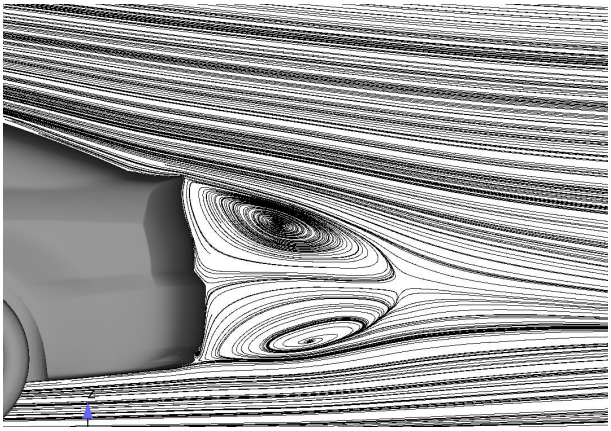

(f) *Velocity streamlines* | *Unsteady*

Figure 4.15: C_p *Rear view & Velocity streamlines* Y_0 | *Smooth underbody* | *Fastback*

While there are no experimental data available for the smooth underbody symmetry line pressure distribution, interesting results are still observed, see figure 4.16. All three methods are very similar except for around the front of the engine under shield, plenum, and front of the roof. Similar as for the baseline the SS method has higher pressure on the roof and lower pressure around the plenum, while the US and SS-EWT methods exhibit similar pressure over the roof. Contrary to the baseline, the SS and US methods exhibit similar behaviour in the front part of the engine under shield while the SS-EWT method generates a low pressure zone.

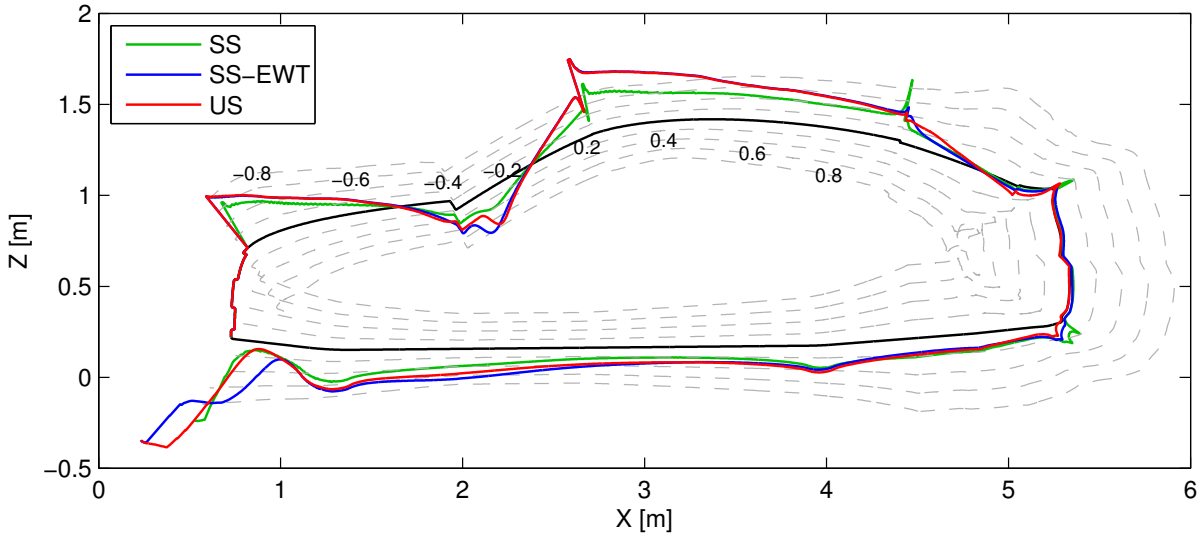

Figure 4.16: C_p *vs* X | *Symmetry line* | *Smooth underbody* | *Fastback*

4.2.2 Smooth underbody | Notchback

The notchback base wake pressure distribution looks very similar as for the fastback with recirculation around the tail lights and bumper for the SS method. The SS-EWT method generates a similar base pressure as the SS method except for a cleaner separation and slightly lower pressure. Furthermore the US method exhibits the same symmetrical recirculation on the sides of the base as for the fastback. Similar behaviour can be seen in pressure measurements from scale model wind tunnel testing at TUB [3].

The same delayed separation on the rear windows as seen in the baseline notchback, see figure 4.6e, can also be observed for the smooth underbody configuration.

Moving on to the velocity streamlines along the symmetry line, see figure 4.6e, all the three methods tend to have top and bottom wake recirculation, while the SS method seem to produce the strongest one. The US and SS-EWT methods have similar behaviour except for the US to be more top biased and the SS-EWT more bottom biased in the recirculation.

Further investigation of the wake using the Z plane velocity streamlines, see figure B.5, show that the US method recirculates closer to the base of the vehicle than the two other methods used. Similarly as for the fastback model. Investigating the X plane total pressure distribution in the same figure, it is evident that the US method exhibits a more compact and realistic wake while the SS and SS-EWT methods generate a very similar flow field to one and another. The two latter methods also generate a more narrow wake when compared to the US method.

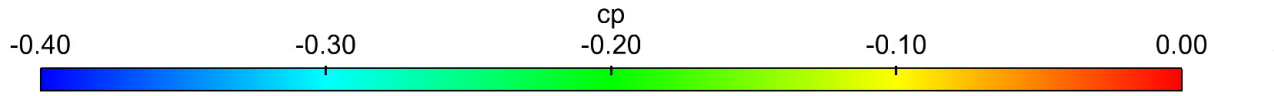

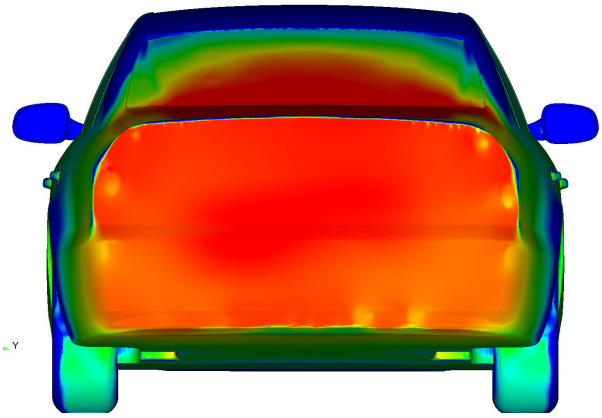

(a) C_p | *Steady*

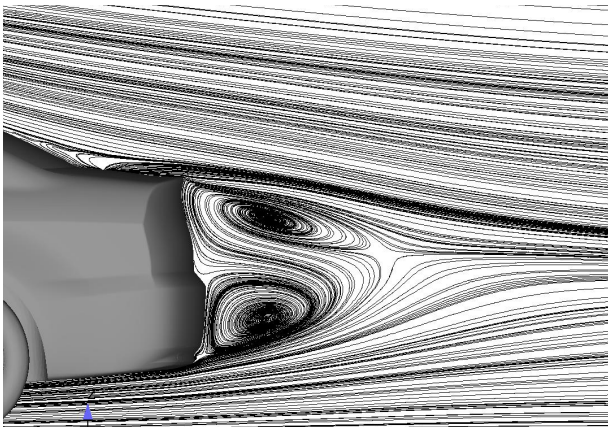

(b) *Velocity streamlines* | *Steady*

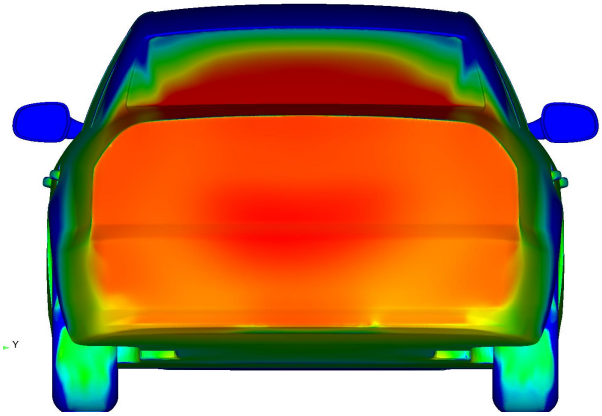

(c) C_p | *Steady EWT*

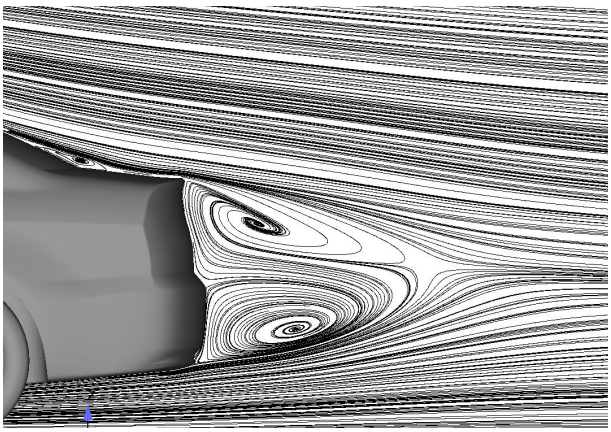

(d) *Velocity streamlines* | *Steady EWT*

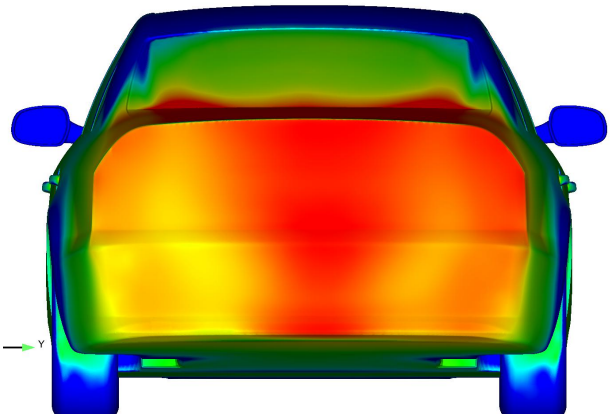

(e) C_p | *Unsteady*

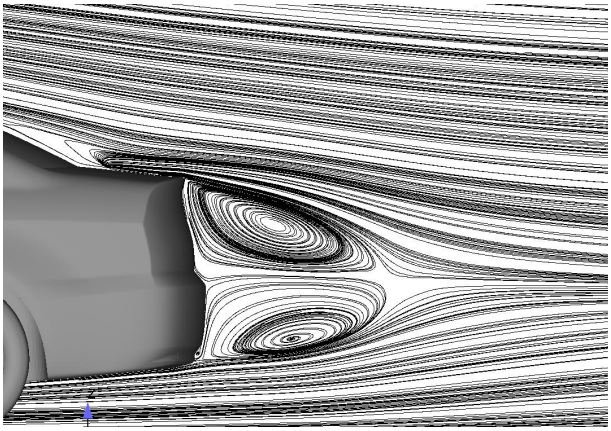

(f) *Velocity streamlines* | *Unsteady*

Figure 4.17: C_p *Rear view & Velocity streamlines* Y_0 | *Smooth underbody* | *Notchback*

Similarly as for the fastback model the symmetry line pressure distribution, see figure 4.18, of all the methods are quite similar with a few exceptions. The US and SS methods have similar behaviour in the front part of the engine under shield, while on the plenum and roof the same deviations as previously observed are exhibited. The SS method predicts a lower pressure near the plenum and higher pressure on the front of the roof when compared to the two other methods. The low pressure zone at the rear window produced by the US method can also be observed in this figure.

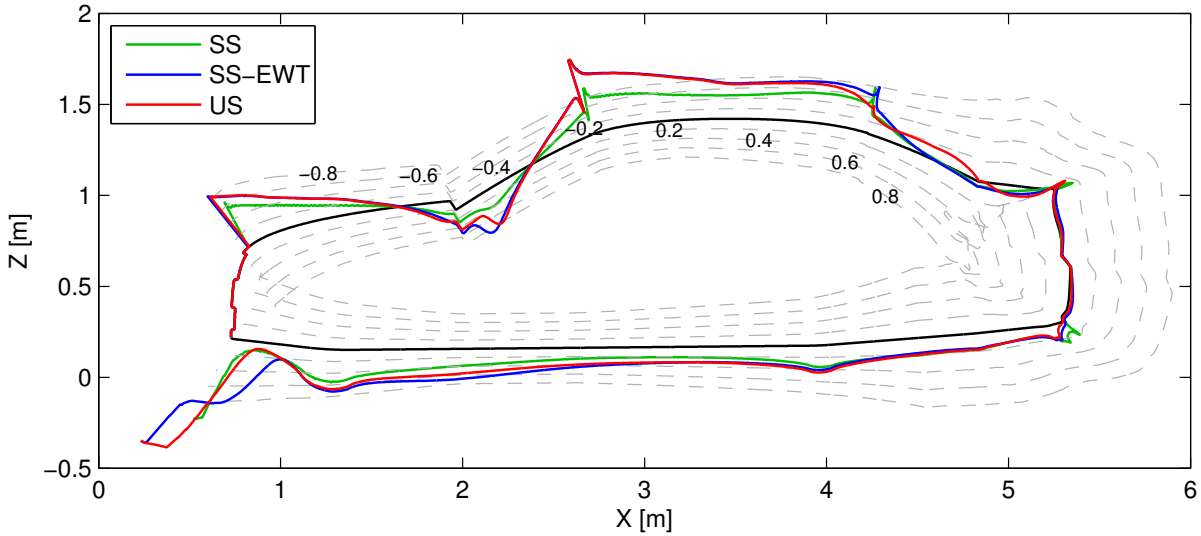

Figure 4.18: C_p *vs* X | *Symmetry line* | *Smooth underbody* | *Notchback*

4.2.3 Smooth underbody | Squareback

Similarly as for the baseline, an great difference of around 50 drag counts can be seen between the US method and both the SS and SS-EWT methods. One reason to this is the difference in base wake pressure, see figure 4.19, the US method has around 100 counts lower pressure coefficient than the SS and SS-EWT methods. Furthermore the flow around the tail lights and bumper tend to recirculate close to the vehicle for the SS and SS-EWT methods.

The symmetry line velocity streamline in figure 4.19 look quite similar for all three methods. The recirculation seems strongest in the bottom part of the SS method and US method, while the SS-EWT method has the same behaviour except less pronounced. The developed vortices in the bottom part of the wake for the US method are very close to the bumper, thus producing the low pressure zone.

The Z plane velocity streamlines in figure B.6 further strengthens the reasoning for the lower base pressure generated by the US method, as a product of the recirculation occurring closer to the vehicle when compared to the two other methods used. The X plane total pressure distributions in the same figure exhibits similar behaviour for all three methods except for the SS method being more disturbed by the wheels in the lowest part of the figure.

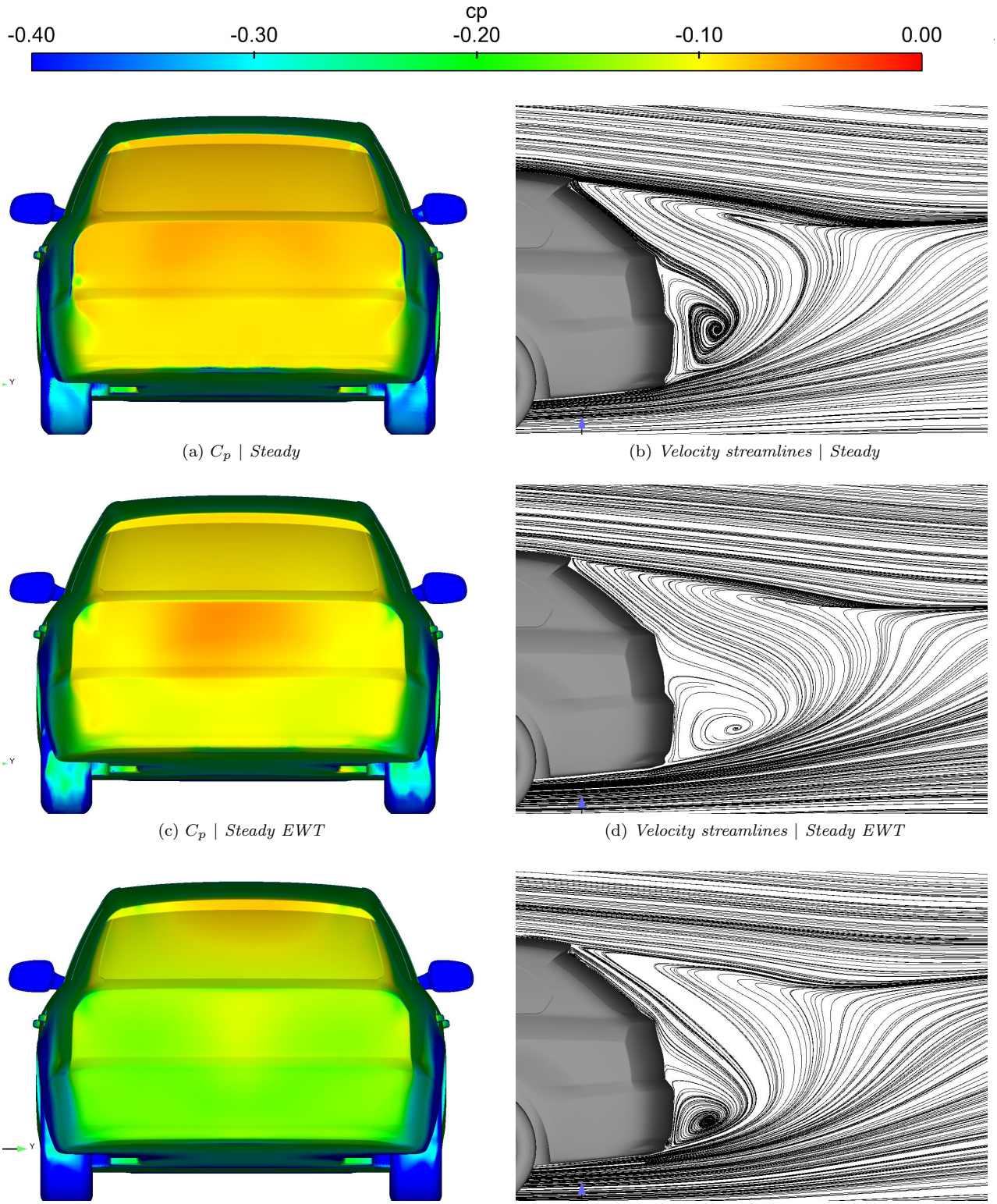

(a) C_p | *Steady*

(b) *Velocity streamlines* | *Steady*

(c) C_p | *Steady EWT*

(d) *Velocity streamlines* | *Steady EWT*

(e) C_p | *Unsteady*

(f) *Velocity streamlines* | *Unsteady*

Figure 4.19: C_p *Rear view & Velocity streamlines* Y_0 | *Smooth underbody* | *Squareback*

Similarly as for the fastback and notchback model the symmetry line pressure distribution, see figure 4.20, of all the methods are quite similar with a few exceptions. The US and SS methods have similar behaviour in the front part of the engine under shield, while on the plenum and roof the same deviations as previously observed are exhibited. The SS method predicts a lower pressure near the plenum and higher pressure on the front of the roof when compared to the two other methods.

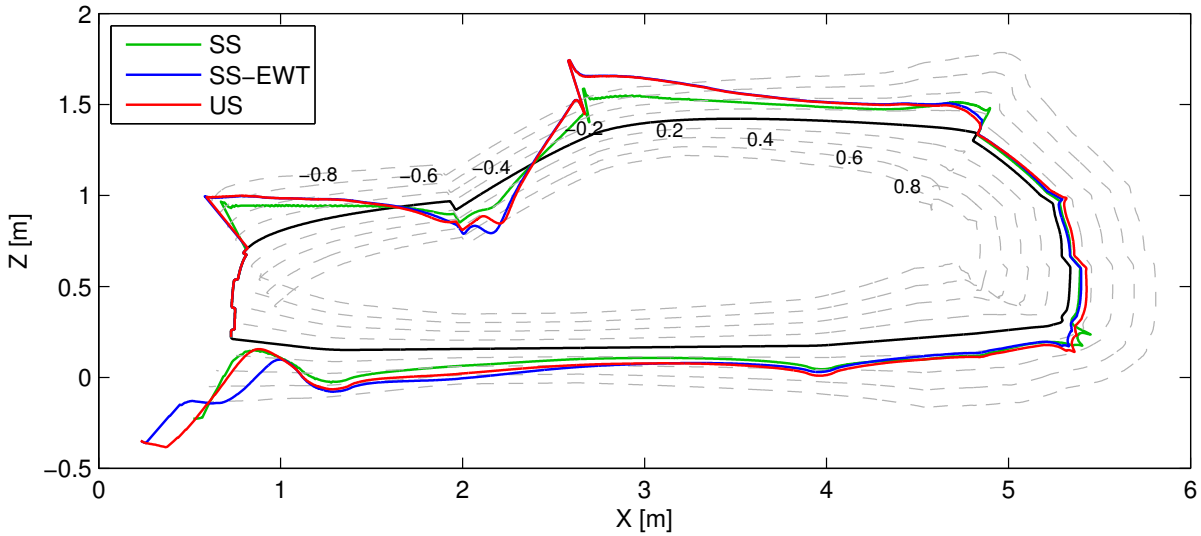

Figure 4.20: C_p *vs* X | *Symmetry line* | *Smooth underbody* | *Squareback*

4.3 Closed body

The experimental data used for closed body is from TUM and thus regarded as not as reliable as the PVT, which is explained in 5.2. In figure 4.10 it can be seen that for the smooth underbody the data from TUM ASME lies around 15 to 20 drag counts above the PVT data, which could mean that the US method correlates very well. This difference can decrease for the closed body since the geometry is simpler.

Due to the lack of industrial usage of the closed body configuration the drag force results will only be presented. The flow field illustrations will be excluded from the report due to their similar behaviour as the smooth underbody configuration.

As for the smooth underbody configurations the US method over predict the drag while the SS and SS-EWT methods under predict the drag, see figure 4.21. The over and under prediction of drag is very similar between the fastback and notchback, where the US method over predicts with 13 to 17 counts and the SS and SS-EWT methods under predict drag with 9 to 16 counts. The squareback model exhibits a larger error for the SS and SS-EWT methods. The US method only over predicts drag with 5 counts while the SS and SS-EWT methods under predict drag with 29 to 37 counts.

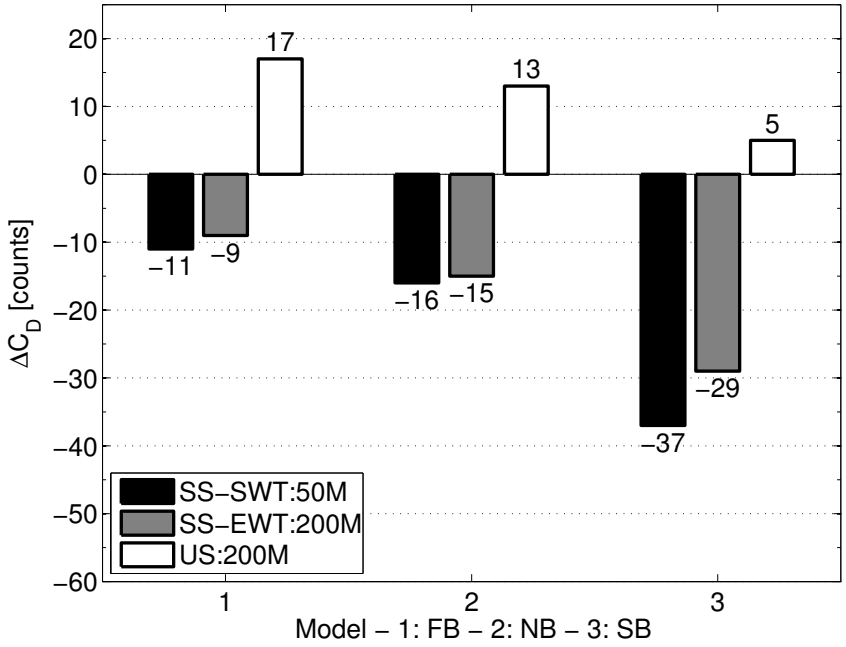

Figure 4.21: ΔC_D | *Closed body* | *REF Exp TUM [2]*

Similarly as for the influence of changing from baseline to smooth underbody configuration, a investigation of changing from baseline to the closed body configuration is made in figure 4.22. The reference data used is the TUM ASME data [2], and is not considered as accurate as the PVT data, see section 5.2.

The fastback and notchback models exhibit similar behaviour, the SS method under predict the drag with 8 counts for the fastback model and 7 counts for the notchback model while the SS-EWT model over predicts the drag with 8 counts for the fastback model and 4 counts for the notchback model. The US method over predict drag with 19 counts for the fastback model and 10 counts for the notchback model. Finally for the squareback model the US method over predicts the drag with 6 counts while the SS-EWT method similarly over predicts the drag with 8 counts. The SS method captures the trend completely and does not deviate.

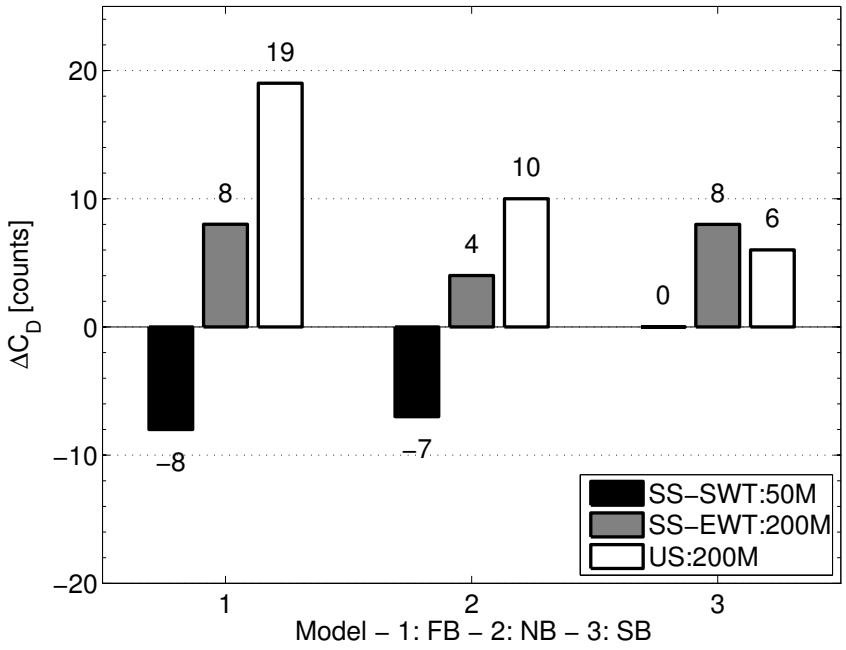

Figure 4.22: ΔC_D | *Influence of Closed body* | *REF Exp TUM [2]*

5 Discussion

To summarise and discuss this work done, the results, error sources, and further work will be discussed in the following sections below.

5.1 Results

The results presented in the previous chapter can be summarised as comparison of absolute drag coefficients, comparison of flow field, and comparison of ability to capture trends. Capturing trends and correct flow field is often regarded as of high importance while comparing absolute values is of equal importance but often have inherit difficulties such as differences in geometry of the domain & wind tunnel. The results in [8] show that when using the US method on open front models, one can expect an drag over prediction of up to 10 to 20 counts when comparing with PVT experiments depending on different cooling configurations. Similar behaviour is seen in this work, although closed front, when investigating the baseline results, see figure 4.2, where the US method over predicts the drag with 21 to 29 counts for the three different models used. Similarly for the smooth underbody configuration, see figure 4.12, the US method over predicts the drag with 7 to 20 counts for the three different models used. The SS-EWT method has the best drag prediction for the baseline configurations, see figure 4.2, with an error of -7 to 6 counts. Investigating the smooth underbody results it can be seen that the US method, see figure 4.12, has the best correlation with the PVT results, with an error of 7 to 20 drag counts.

To further evaluate the results, the trends illustrated in figure 4.14 are further investigated. The figure illustrates the drag difference between changing from baseline to smooth underbody for the different numerical results with the PVT data as reference. The results are quite clear where the US method has the best ability to capture this trend, with an drag under prediction of 9 to 14 counts for the three different models used. The SS-EWT method has an drag under prediction of 19 to 21 counts and the SS method 29 to 34 drag counts. A Similar comparison is done for the difference between baseline and closed body in figure 4.22. The experimental data used is from this work done at TUM [2] and thus not as reliable as the PVT data, which is further discussed in section 5.2. While its difficult to say which method behaves the best in these results, it can be seen that the SS-EWT method is the most consistent with an drag over prediction of 4 to 8 counts.

To further investigate the flow field and compare it to experimental results, the symmetry line pressure distribution is observed. Figures 4.5, 4.7, and 4.9 show that the the US method has best correlation to the pressure measurements from TUM [1]. The SS-EWT method results are very similar to the US method except for some areas in the middle of the underbody where the US method seem to better capture the pressure. The plenum, beginning of the windscreen, end of rear window are areas where all three methods over predict the pressure while the front of the under body and base are areas where all three models under predict the pressure.

There is a clear distinction between the flow field of the SS and SS-EWT methods, and the US method. The flow field generated by the SS and SS-EWT methods consistently exhibits a more sporadic flow when compared to the US method. The US method exhibits a more compact flow for all configurations and has a more realistic non-sprawling pattern, based on surface and wake measurements from [1, 3, 4]. The US method has a inherit advantage when simulating turbulent flow since the flow is fluctuating, this is one of the possible reasons to the great difference in flow field behaviour presented.

5.2 Error sources

When comparing experimental and numerical data it is important to investigate possible sources of error. One important factor is the geometrical representation. Starting of by comparing the geometry used in this work to the geometry used in the PVT data. There are only two differences if one disregards possible manufacturing tolerance errors, they are wheels and suspension assembly. The wheels used in the PVT data set are production wheels, see figure 5.1b that are similar to the DrivAer wheels, see figure 5.1a. The difference is how the spokes are angled, while the amount of spokes and general shape of them are the same. The size of tire and rim is very similar as the DrivAer wheels. The model used in this work has slick tires while the PVT data set uses normal threaded tires. Furthermore the model used in the PVT data set has wheel hubs, brake discs, and a-arms to hold the wheels in place while the DrivAer model published at the time of this work has no suspension or hub components at all. The sum of this introduces some uncertainty in the results and 3D printed wheels were tested to reduce the uncertainty. The tests were performed without the ground simulation system since the 3D printed plastic wheels are not load bearing. For the baseline configurations the affect of changing from the PVT wheels to the DrivAer wheels, see figure 5.1, was an drag reduction of 3 to 4 counts for the three different models.

(a) *DrivAer model wheels*

(b) *PVT model wheels*

Figure 5.1: *Geometrical differences | Wheels PVT*

Comparing the geometry used in this work with the geometry used in the scale model testing at TUM [1, 2], the same differences as the PVT data set are also seen here. The only difference being that the wheels used during the experiments at TUM differ quite alot compared to the original model. The wheels used consist of disc wheels with ten holes drilled through them, they can be seen in in figure 5.2a. Significantly less air can pass through the wheels used at TUM compared to the DrivAer models wheels, which can impact the results [11]. Furthermore the scale model wind tunnel uses stings to mount the wheels and car, which can have a impact on the flow field by increasing the drag by up to 4 counts and lift of up to 15 counts [12].

The illustrations used from TUB [3, 4] are only used for visual comparison. It is important to note that the wind tunnel at TUB does not use a moving ground system, see figure 5.2b, which will impact the results to some extent.

(a) *TU München | Setup*

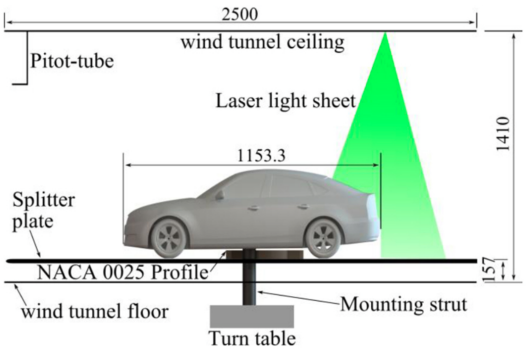

(b) *TU Berlin | Setup*

Figure 5.2: *Geometrical differences and setups | Scale models*

5.3 Further work

In order to better compare the numerical results to experimental results, surface pressure measurements and wake measurements in a full scale wind tunnel is suggested for further work. This is due to the high importance of comparing flow fields and trends instead of only absolute values. Flow visualisation paint, smoke, and tufts could also be used to further understand the flow field and compare it.

Further development of the mesh strategy and experimentation with different turbulence models would be of great interest since the SS-EWT method has decent performance, using a mesh designed for the US method originally. Further optimisation of the mesh for the chosen steady method could improve upon the results.

Open front simulations and experiments would be a natural proceeding step due to the fact that production vehicles are using open front configurations. The relative simple engine compartment created by TUM [1], should not prove difficult to implement in the numerical methods used in this work. The work done in [8] has reached good results using the US method on open front configurations with a consistency in the prediction of drag, even though over predicted, and good correlation between the flow fields.

6 Conclusions

Reflecting upon the purpose stated in section 1.1, there are several questions to be answered regarding the different numerical methods evaluated in the scope of this work. The baseline configuration is of greatest interest for industry applications since it has the most resemblance to production vehicles, while the smooth underbody configuration should not be neglected. The closed body configurations lacks industry applications and has been limited by the amount of experimental data available. Based on the baseline and smooth underbody configurations the US method can be considered the method which can capture the most realistic flow field and has the best ability to capture trends for both the configurations. The SS-EWT method proved the best drag prediction for the baseline model while the US method had a quite consistent drag over prediction, as seen in [8]. Furthermore the US method had the best drag prediction for the smooth underbody and if one were to choose only one method for further work it would be the US method. This based on the ability to generate a more realistic flow field, correlation with surface pressure measurements, and overall good ability for capturing trends and absolute drag values to some extend.

There are significant differences in the computational effort required for the different methods used. The US method takes 30 to 40 times longer to solve than the SS-EWT method. This means that if short lead times are of great importance, the SS-EWT method could be further developed for this use. The difference in solving time will most likely be reduced in the near future based on the expansion rate of cluster capacity in the industry. For example interpolating results between different configurations has a very positive impact in the US method and can reduce the computational time by 25%. Furthermore the quality of mesh has a great impact on the convergence rate of the US method, which was observed when comparing the smooth underbody and closed body configurations to the baseline configuration.

A Underbody configurations

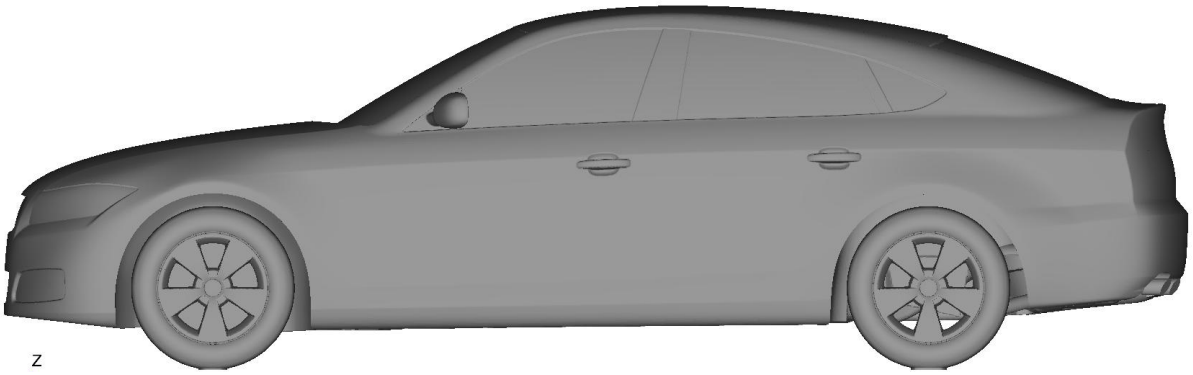

(a) *Baseline* | *Side view*

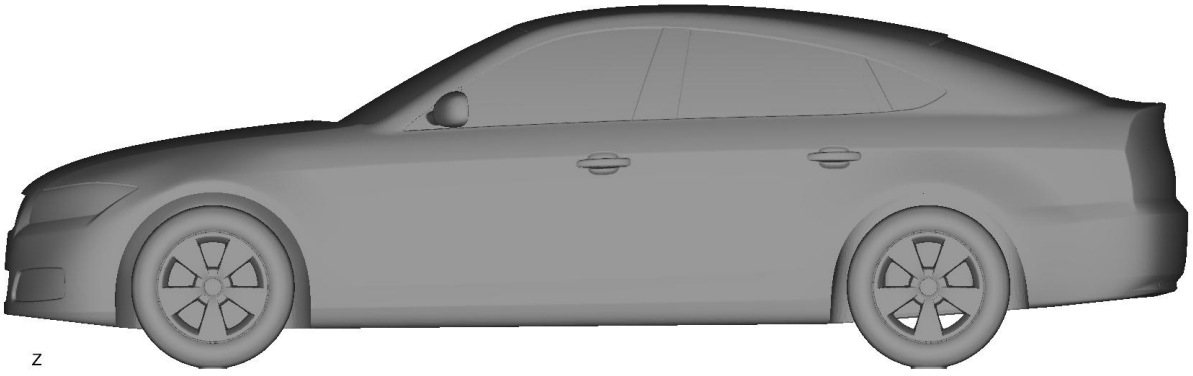

(b) *Smooth underbody* | *Side view*

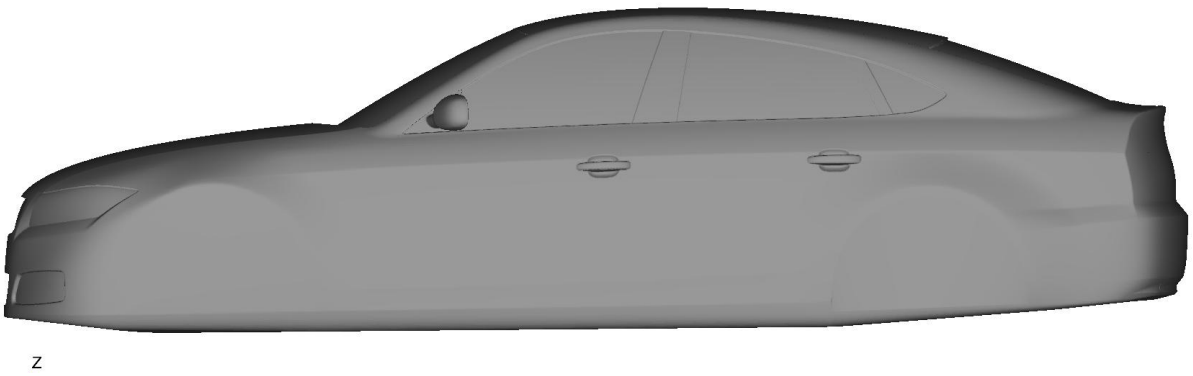

(c) *Closed body* | *Side view*

Figure A.1: *Underbody configurations* | *Side view*

B Wake illustrations

B.1 Baseline

B.1.1 Baseline | Fastback

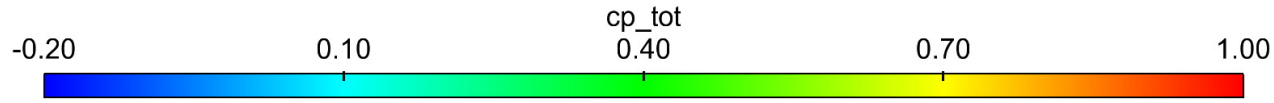

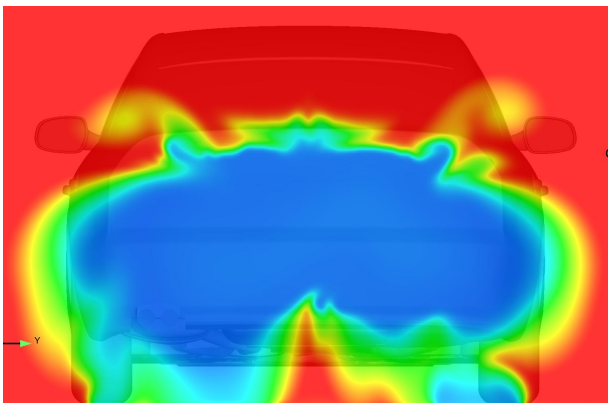

(a) C_{p-tot} | *Steady*

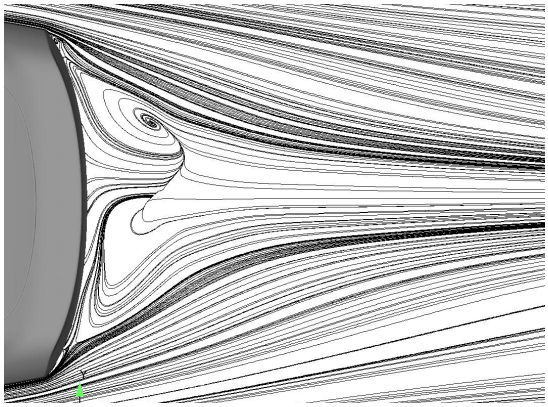

(b) *Velocity streamlines* | *Steady*

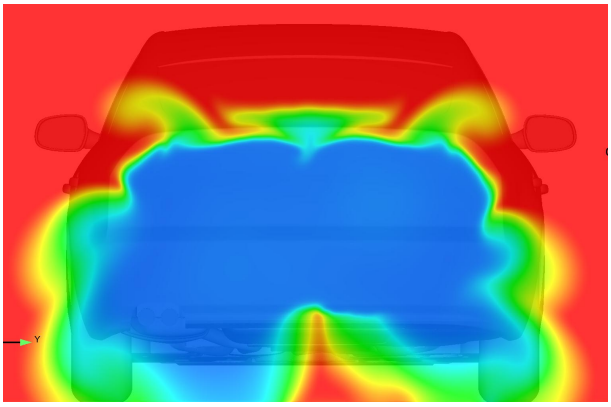

(c) C_{p-tot} | *Steady EWT*

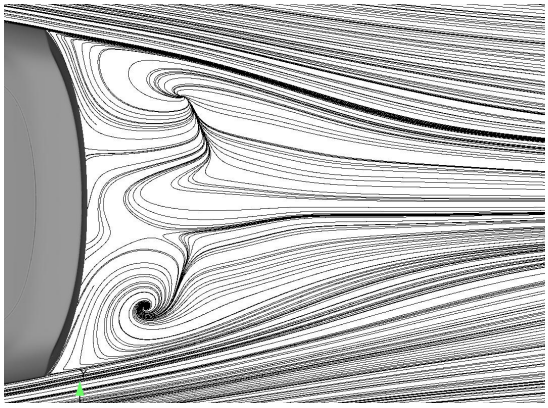

(d) *Velocity streamlines* | *Steady EWT*

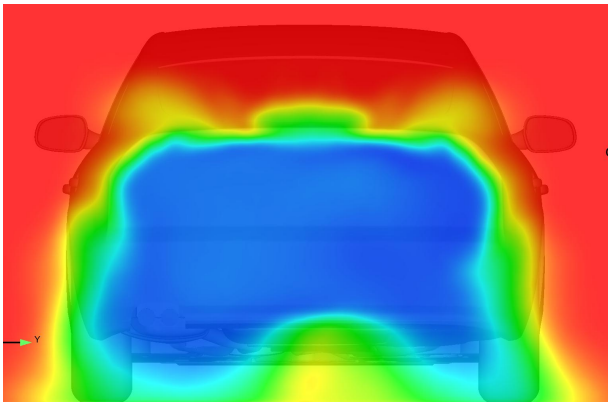

(e) C_{p-tot} | *Unsteady*

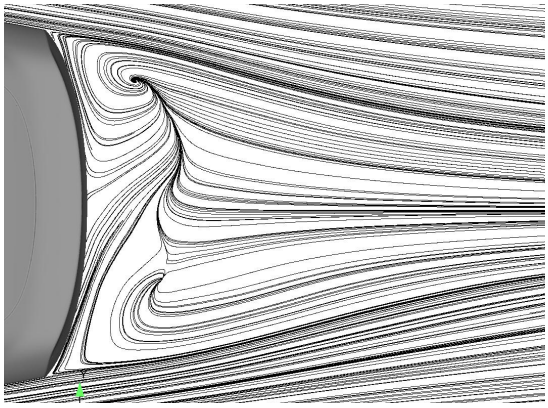

(f) *Velocity streamlines* | *Unsteady*

Figure B.1: C_{p-tot} *Rear view* $0.1m$ *behind car & Velocity streamlines* $Z = 0.824m$ | *Baseline* | *Fastback*

B.1.2 Baseline | Notchback

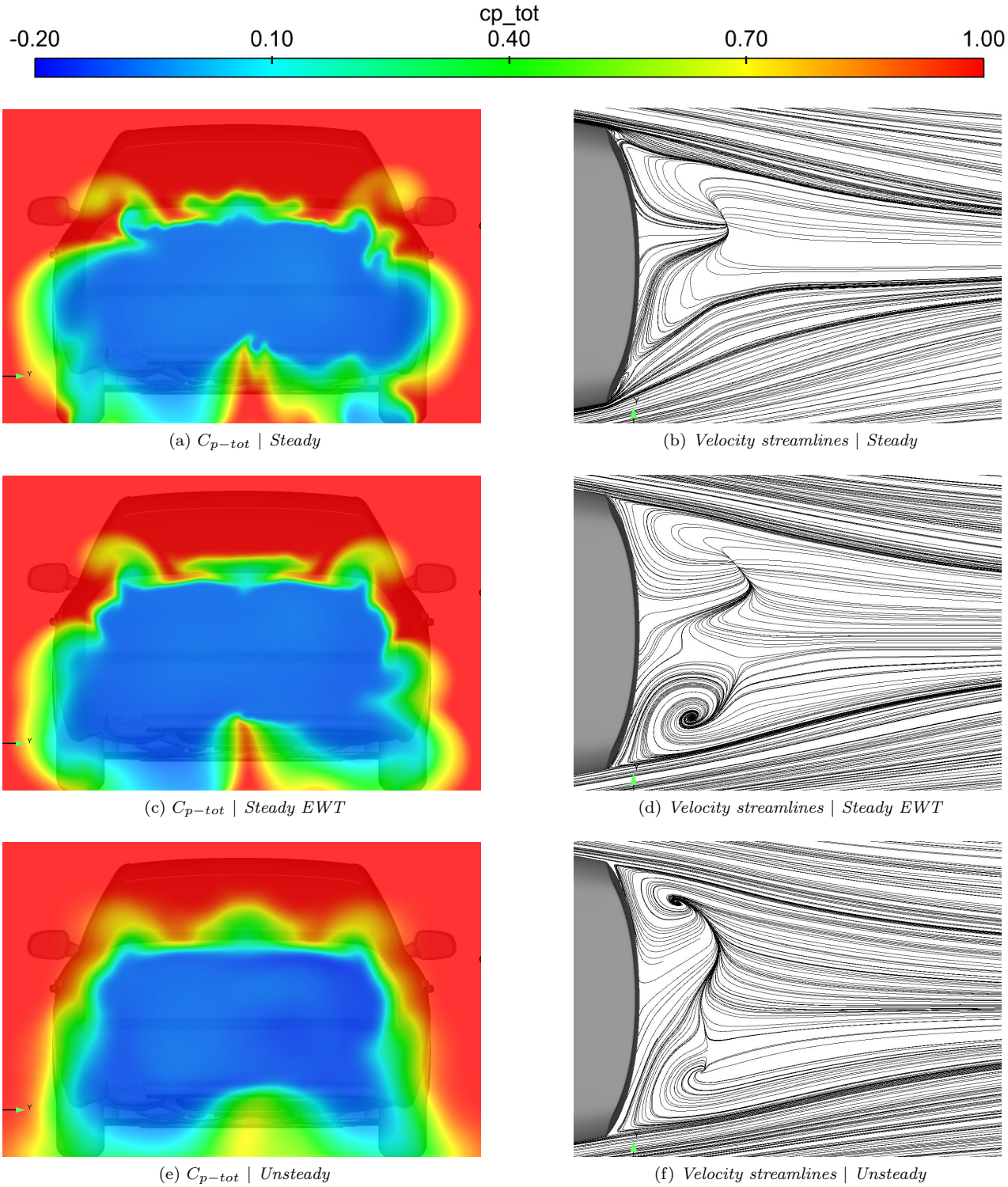

(a) C_{p-tot} | *Steady*

(b) *Velocity streamlines* | *Steady*

(c) C_{p-tot} | *Steady EWT*

(d) *Velocity streamlines* | *Steady EWT*

(e) C_{p-tot} | *Unsteady*

(f) *Velocity streamlines* | *Unsteady*

Figure B.2: C_{p-tot} *Rear view* $0.1m$ *behind car & Velocity streamlines* $Z = 0.824m$ | *Baseline* | *Notchback*

B.1.3 Baseline | Squareback

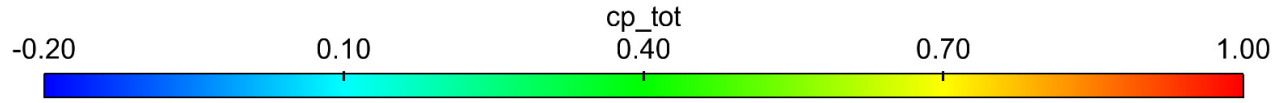

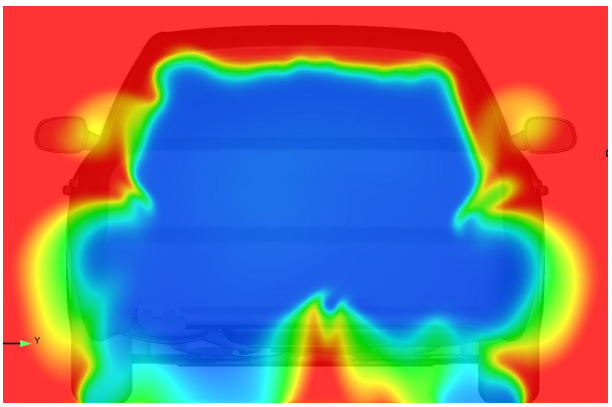

(a) C_{p-tot} | *Steady*

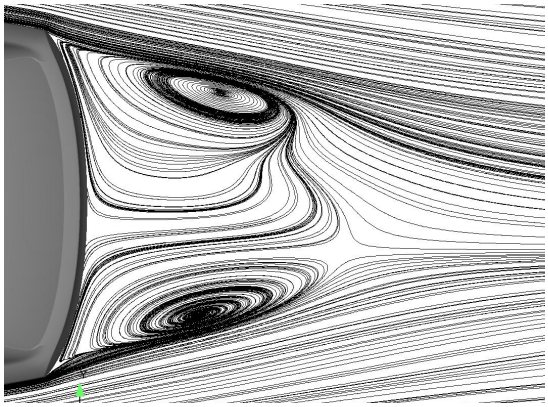

(b) *Velocity streamlines* | *Steady*

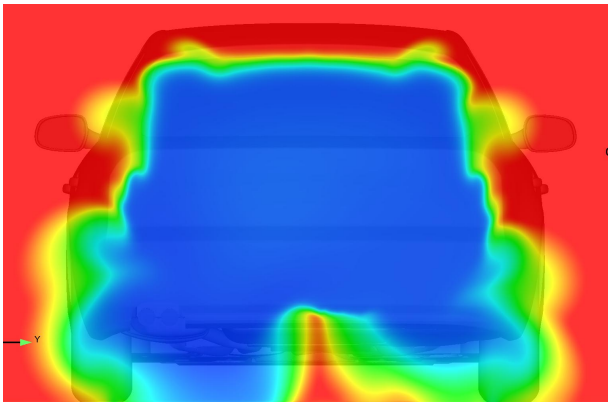

(c) C_{p-tot} | *Steady EWT*

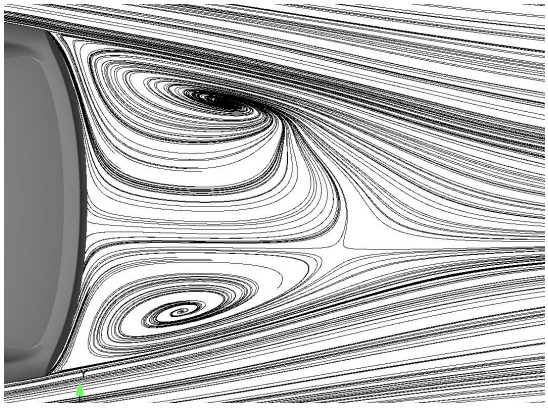

(d) *Velocity streamlines* | *Steady EWT*

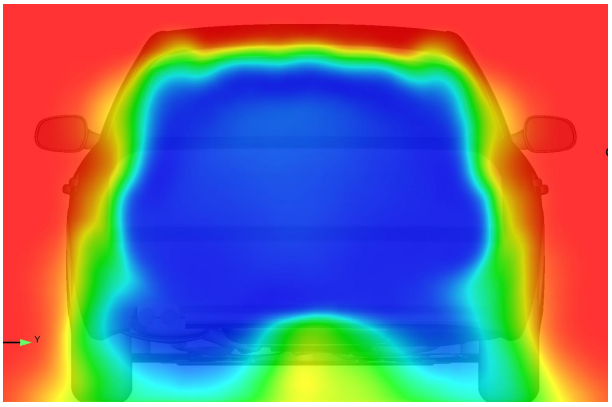

(e) C_{p-tot} | *Unsteady*

(f) *Velocity streamlines* | *Unsteady*

Figure B.3: C_{p-tot} *Rear view* $0.1m$ *behind car & Velocity streamlines* $Z = 0.824m$ | *Baseline* | *Squareback*

B.2 Smooth underbody

B.2.1 Smooth underbody | Fastback

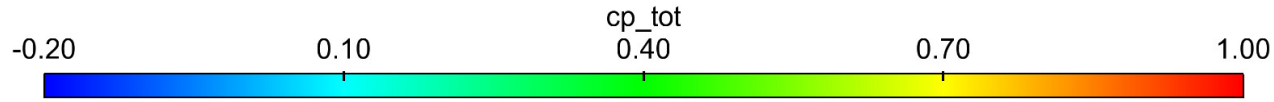

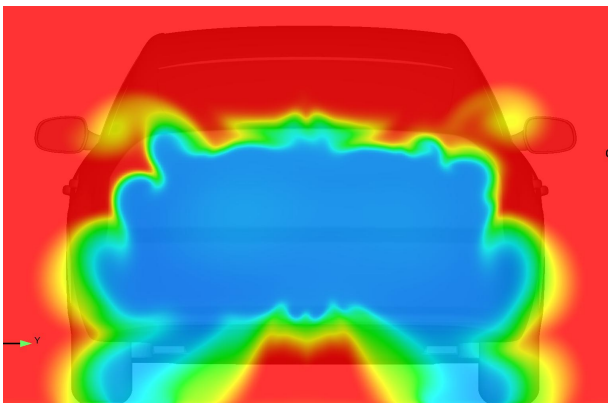

(a) C_{p-tot} | *Steady*

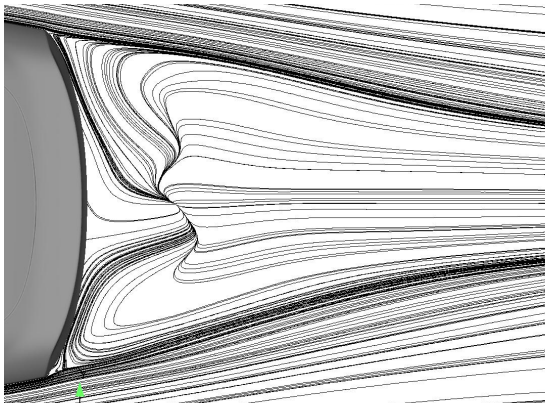

(b) *Velocity streamlines* | *Steady*

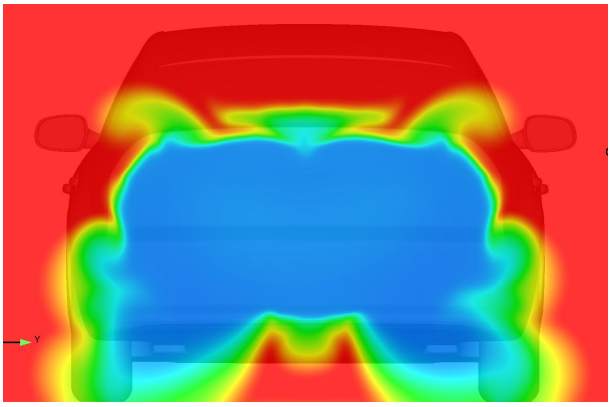

(c) C_{p-tot} | *Steady EWT*

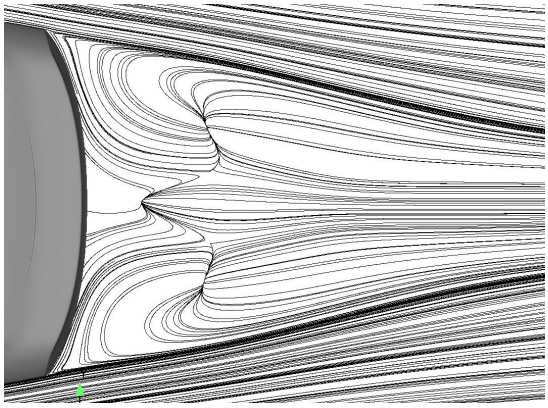

(d) *Velocity streamlines* | *Steady EWT*

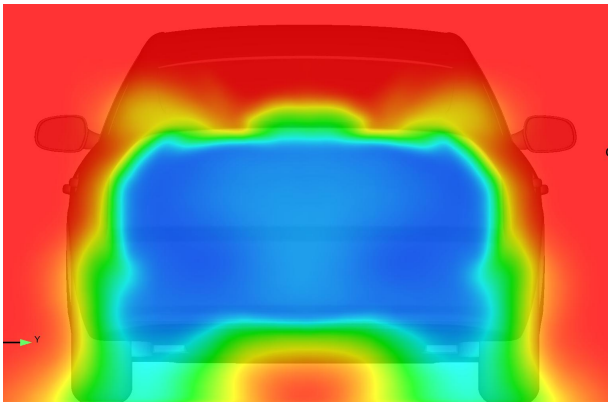

(e) C_{p-tot} | *Unsteady*

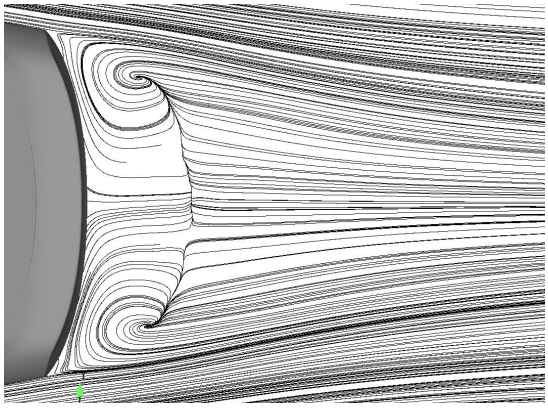

(f) *Velocity streamlines* | *Unsteady*

Figure B.4: C_{p-tot} *Rear view* $0.1m$ *behind car & Velocity streamlines* $Z = 0.824m$ | *Smooth underbody* | *Fastback*

B.2.2 Smooth underbody | Notchback

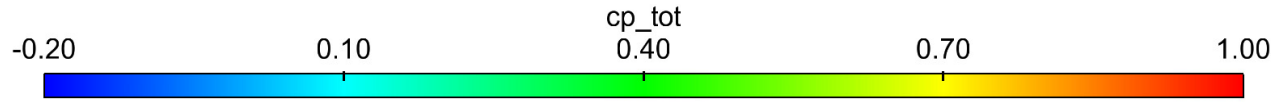

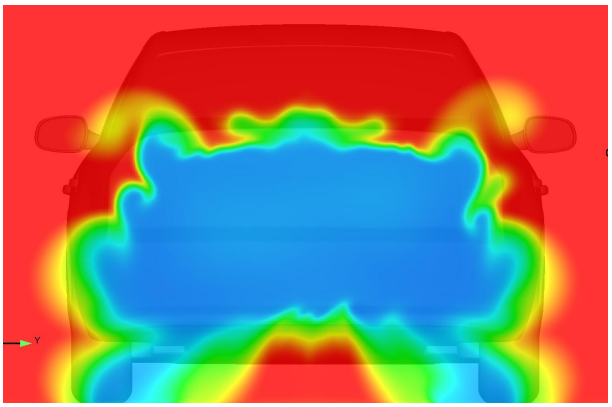

(a) C_{p-tot} | *Steady*

(b) *Velocity streamlines* | *Steady*

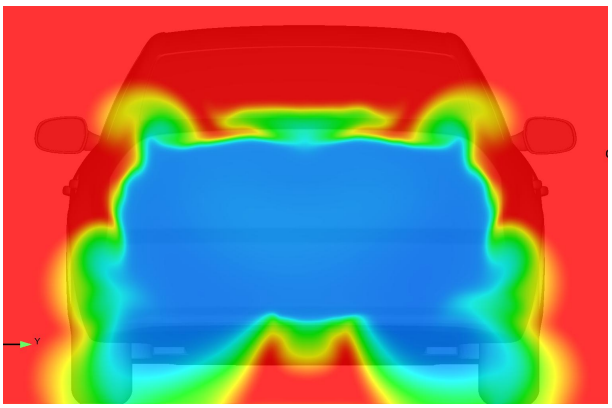

(c) C_{p-tot} | *Steady EWT*

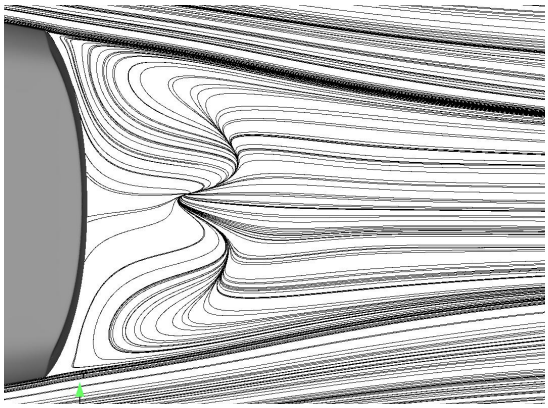

(d) *Velocity streamlines* | *Steady EWT*

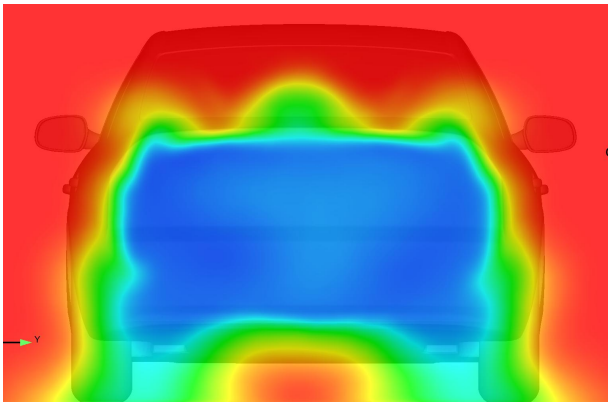

(e) C_{p-tot} | *Unsteady*

(f) *Velocity streamlines* | *Unsteady*

Figure B.5: C_{p-tot} *Rear view* $0.1m$ *behind car & Velocity streamlines* $Z = 0.824m$ | *Smooth underbody* | *Notchback*

B.2.3 Smooth underbody | Squareback

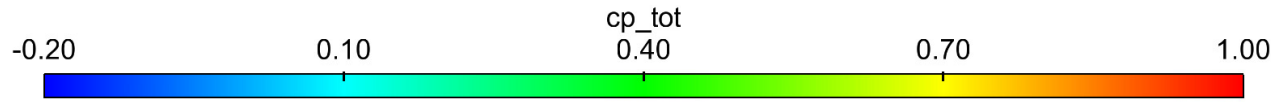

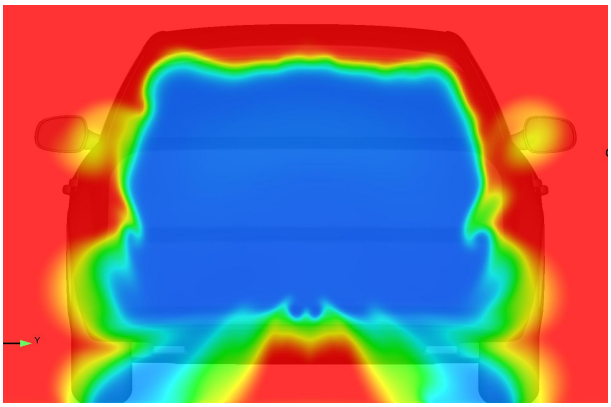

(a) C_{p-tot} | *Steady*

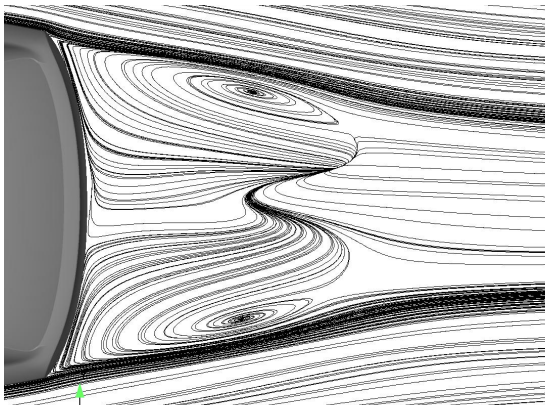

(b) *Velocity streamlines* | *Steady*

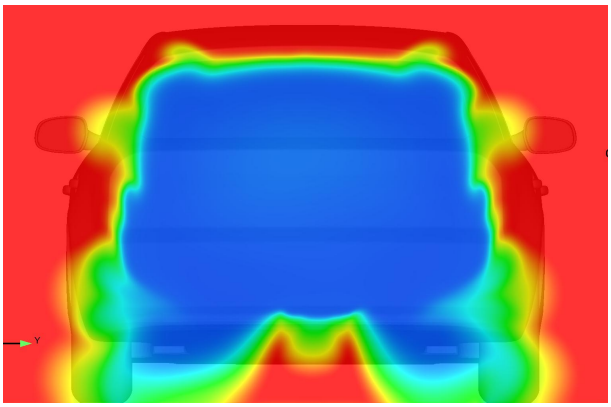

(c) C_{p-tot} | *Steady EWT*

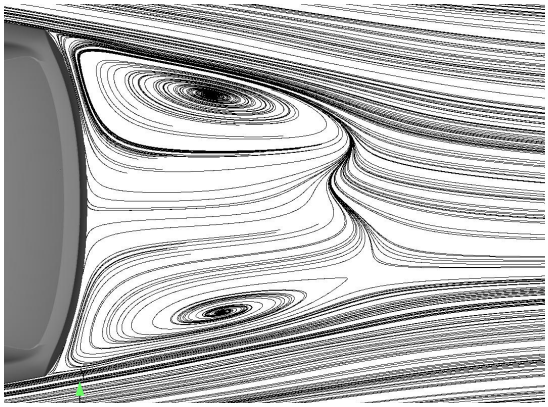

(d) *Velocity streamlines* | *Steady EWT*

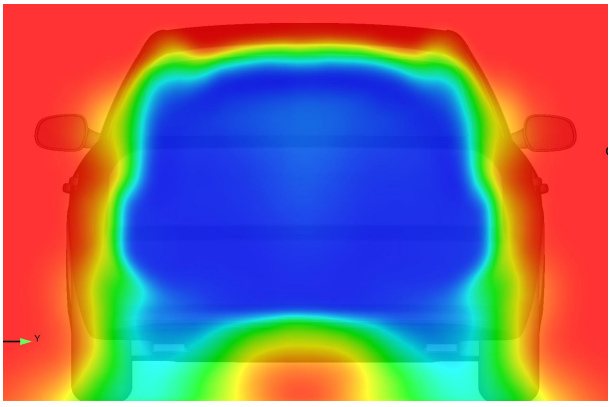

(e) C_{p-tot} | *Unsteady*

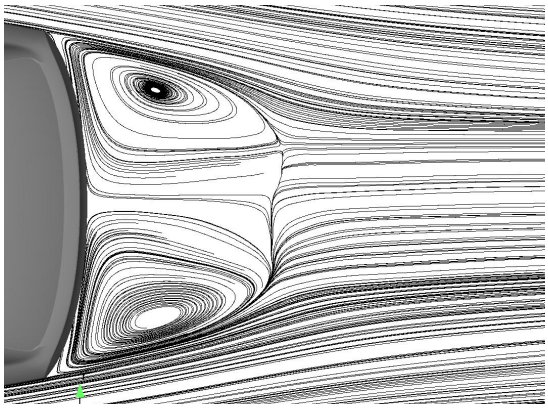

(f) *Velocity streamlines* | *Unsteady*

Figure B.6: C_{p-tot} *Rear view* $0.1m$ *behind car & Velocity streamlines* $Z = 0.824m$ | *Smooth underbody* | *Squareback*

References

[1] A. I. Heft, T. Indinger, and N. A. Adams. "Introduction of a New Realistic Generic Car Model for Aerodynamic Investigations". *SAE Technical Paper*. SAE International, Apr. 2012. DOI: 10.4271/2012-01-0168.

[2] S. Mack et al. "The Interior Design of a 40% Scaled DrivAer Body and First Experimental Results". *ASME Technical Paper*. ASME, July 2012. DOI: 10.1115/FEDSM2012-72371.

[3] D. Wieser et al. Experimental Comparison of the Aerodynamic Behavior of Fastback and Notchback DrivAer Models. *SAE Int. J. Passeng. Cars - Mech. Syst.* **7** (Apr. 2014), 682–691. DOI: 10.4271/2014-01-0613.

[4] C. Strangfeld et al. "Experimental Study of Baseline Flow Characteristics for the Realistic Car Model DrivAer". *SAE Technical Paper*. SAE International, Apr. 2013. DOI: 10.4271/2013-01-1251.

[5] N. Ashton and A. Revell. "Comparison of RANS and DES methods for the DrivAer automotive body". *SAE Technical Paper*. SAE International, Apr. 2015. DOI: 10.4271/2015-01-1538.

[6] B. C. Peters et al. "Simulating DrivAer with Structured Finite Difference Overset Grids". *SAE Technical Paper*. SAE International, Apr. 2015. DOI: 10.4271/2015-01-1536.

[7] *Calculation Procedure AEDCAE01. Aerodynamic Performance Assesment of a Car Exterior With a Closed Front*. Volvo Car Corporation, 2012.

[8] L. Sterken et al. Numerical implementation of Detached Eddy Simulation on a passenger vehicle and some experimental correlation. *ASME J. Fluids Eng.* (2015).

[9] P. Spalart et al. A New Version of Detached-eddy Simulation, Resistant to Ambiguous Grid Densities. English. *Theoretical and Computational Fluid Dynamics* **20**.3 (2006), 181–195. ISSN: 0935-4964. DOI: 10.1007/s00162-006-0015-0.

[10] J. Sternéus, T. Walker, and T. Bender. "Upgrade of the Volvo Cars Aerodynamic Wind Tunnel". *SAE Technical Paper*. SAE International, Apr. 2007. DOI: 10.4271/2007-01-1043.

[11] Z. Qui. "Wheel Aerodynamic Developments by Module-based Prototype Rims and Stationary Rim shield". Master thesis. Chalmers University of Technology, 2009.

[12] B. Hetherington and D. B. Sims-Williams. "Wind Tunnel Model Support Strut Interference". *SAE Technical Paper*. SAE International, Mar. 2004. DOI: 10.4271/2004-01-0806.